Biometrics 000, 000–000 DOI: 000
000 0000

Post-Selection Inference for Changepoint Detection Algorithms with Application to Copy Number Variation Data

Sangwon Hyun*

Department of Data Sciences and Operations, University of Southern California, Los Angeles, CA.

email: shyun@usc.edu

and

Kevin Z. Lin

Department of Statistics, University of Pennsylvania, Philadelphia, PA.

and

Max G'Sell and Ryan J. Tibshirani

Department of Statistics and Data Science, Carnegie Mellon University, Pittsburgh, PA.

Summary: Changepoint detection methods are used in many areas of science and engineering, e.g., in the analysis of copy number variation data to detect abnormalities in copy numbers along the genome. Despite the broad array of available tools, methodology for quantifying our uncertainty in the strength (or presence) of given changepoints *post-selection* are lacking. Post-selection inference offers a framework to fill this gap, but the most straightforward application of these methods results in low-powered hypothesis tests and leaves open several important questions about practical usability. In this work, we carefully tailor post-selection inference methods towards changepoint detection, focusing on copy number variation data. To accomplish this, we study commonly used changepoint algorithms: binary segmentation, as well as two of its most popular variants, wild and circular, and the fused lasso. We implement some of the latest developments in post-selection inference theory, mainly auxiliary randomization. This improves the power, which requires implementations of MCMC algorithms (importance sampling and hit-and-run sampling) to carry out our tests. We also provide recommendations for improving practical useability, detailed simulations, and example analyses on array CGH as well as sequencing data.

Key words: CGH analysis; changepoint detection; Copy number variation; Hypothesis tests; Post-selection inference; Segmentation algorithms

This paper has been submitted for consideration for publication in *Biometrics*

1. Introduction

Changepoint detection algorithms identify changes in data distribution along a sequence of observations, and is commonly used in copy number variation (CNV) analyses the detect deviations in the copy number in any region along the genome (Zhang, 2010). Specifically, in this article, we study the canonical changepoint model, where changes occur only in the mean. Let the vector $\boldsymbol{Y} = (Y_1, \ldots, Y_n) \in \mathbb{R}^n$ be a data vector with independent Gaussian entries,

$$Y_i \sim \mathcal{N}(\theta_i, \sigma^2), \quad i = 1, \ldots, n, \tag{1}$$

where the unknown mean vector $\boldsymbol{\theta} \in \mathbb{R}^n$ forms a piecewise constant sequence. That is, for locations $1 \leqslant b_1 < \cdots < b_t \leqslant n-1$,

$$\theta_{b_j+1} = \ldots = \theta_{b_{j+1}}, \quad j = 0, \ldots, t.$$

where for convenience we write $b_0 = 0$ and $b_{t+1} = n$. We call $b_1, \ldots, b_t$ *changepoint* locations of $\boldsymbol{\theta}$. Given such models, changepoint detection algorithms typically focus on estimating the number of changepoints t (possibly none), as well as the locations $b_1, \ldots, b_t$, from a single vector $\boldsymbol{Y}$. This includes *binary segmentation* (BS) and its many variants common in the literature, such as *wild binary segmentation* (WBS, Fryzlewicz (2014)) and *circular binary segmentation* (CBS, Olshen et al. (2004)). Loosely speaking, these algorithms estimate the changepoint locations by scanning the entire vector Y and finding locations where the empirical means to the left and right segment are well separated. Despite the large number of theoretical results that formalize the point-wise estimation performance of these algorithms (see Lin et al. (2017) and references within), there has been much fewer works that focus on computing valid p-values that quantify the significance of such changepoints. Having valid p-values can be greatly beneficial for filtering changepoints in an automated fashion, where only statistically significant changepoints are kept for potential downstream analyses. As we show later in this section, this methodological gap can be problematic

for CNV analyses since naive hypothesis tests can inflate the Type-I error, leading to undesirable filtering procedures. Hence, in this article, we leverage the recent developments in post-selection inference (Tibshirani et al., 2018) to develop an downstream algorithm to compute p-values within this framework for the aforementioned changepoint algorithms. By developing valid downstream inferential tools, we strengthen commonly-used changepoint detection algorithms in CNV analyses by enabling a principled way to filter changepoints in an automated fashion.

We provide a high-level summary of the post-selection inference applied to changepoint model (1). This serves both as an overview of the post-selection framework and also highlights the algorithmic challenges we resolve in article. The machinery that we build off is developed in works like Fithian et al. (2014, 2015); Tian and Taylor (2018), whose results we rely on.

Basic inference procedure. The basic inference procedure we consider is as follows.

(1) Given data $\boldsymbol{Y}$, apply a changepoint algorithm to detect some fixed number of changepoints k. Denote the estimated changepoint locations by $\widehat{b}_1, \ldots, \widehat{b}_k$, and their respective changepoint directions (whether the estimated change in mean was positive or negative) by $\widehat{d}_1, \ldots, \widehat{d}_k \in \{-1, 1\}$. Let $\boldsymbol{I}_1, \ldots, \boldsymbol{I}_{k+1}$ denote the partition of $\{1, \ldots, n\}$ formed by $\widehat{\boldsymbol{b}}_{1:k}$. The specifics of the changepoint algorithms that we consider are given in Section 2.1.

(2) Form contrast vectors $\boldsymbol{v}_1, \ldots, \boldsymbol{v}_k \in \mathbb{R}^n$, defined so that for arbitrary $\boldsymbol{y} \in \mathbb{R}^n$,

$$\boldsymbol{v}_j^T \boldsymbol{y} = \widehat{d}_j \cdot \Big\{ \frac{1}{|\boldsymbol{I}_{j+1}|} \Big(\sum_{i \in \boldsymbol{I}_{j+1}} \boldsymbol{y}_i \Big) - \frac{1}{|\boldsymbol{I}_j|} \Big(\sum_{i \in \boldsymbol{I}_j} \boldsymbol{y}_i \Big) \Big\}, \tag{2}$$

for $j = 1, \ldots, k$ where $|\boldsymbol{I}_j|$ denotes the cardinality of the set $\boldsymbol{I}_j$. Hence, $\boldsymbol{v}_j^T \boldsymbol{Y}$ represents the difference between the sample means of segments to right and left of $\widehat{b}_j$,

(3) For each $j = 1, \ldots, k$, we test the hypothesis $H_0 : \boldsymbol{v}_j^T \boldsymbol{\theta} = 0$ by rejecting for large values of a statistic $T(\boldsymbol{Y}, \boldsymbol{v}_j)$, which is computed based on knowledge of the changepoint algorithm that produced $\widehat{\boldsymbol{b}}_{1:k}$ in Step 1, the desired contrast vector (2) formed in Step 2, and the

value of σ^2. Each statistic yields a p-value under the null (assuming the model (1)). The details of $T(\boldsymbol{Y}, \boldsymbol{v}_j)$ are given in Sections 2.2 and 3.

(4) Optionally, we can use Bonferroni correction by multiplying the p-values by k, to account for multiplicity.

It is worth mentioning that several variants of this basic procedure are possible. For example, σ^2 can either be estimated from an alternative dataset or left unspecified; the number of changepoints k in Step 1 can be estimated from data; alternative contrast vectors to (2) in Step 2 may be used to measure more localized mean changes. We dedicate the following sections to highlight the novelties of our work within the simplified framework prescribed above, and defer discussions of such variants to the Appendix. Additionally, though not covered in our article, the p-values from our tests can be inverted to form confidence intervals for population contrasts $\boldsymbol{v}_j^T\boldsymbol{\theta}$ for $j = 1, \ldots, k$ (Tibshirani et al., 2018).

Contributions. Our article has two primary contributions. First, we specialize the existing post-selection inference framework for CNV analyses in order to filter estimated changepoints, and show their versatility on array-CGH and sequencing data (Section 4). We prove results to facilitate concrete algorithms and provide extensive guidelines and variants that can be helpful for researchers. Second, we develop new methodologies to improve the power of our inferential tools, and verify this improvement by simulation.

1.1 *CNV background and motivating analysis*

To motivate the necessity for valid inferential tools in changepoint detection, we present a motivating CNV analysis on array comparative genomic-hybridization (aCGH) data. Broadly speaking, CNV analyses investigate the structural variation of the genome where the total copy number of particular large regions in a chromosome deviate from two, the expected copy number – one from each parental cell. This type of variation has been implicated with tumor progression, and therefore many studies use CNV analyses to identify which regions of the

genome to specifically investigate in future analyses (see works like Zhang (2010)). Towards this end, aCGH data is one of many types of data frequently collected to study CNV. This type of data is collected by microarrays, where the $\log_2$ copy number ratio between case and control cells along different regions along the genomes is measured by probes. However, since these measurements are often quite noisy, changepoint detection algorithms need to be used on aCGH data for effective detection of regions of CNV. The data in this motivating analysis originates from Snijders et al. (2001), which studies the CNV of fibroblast cell lines, and is a common benchmark dataset for many changepoint detection algorithms, such as Olshen et al. (2004) and Duy et al. (2020).

Figure 1 illustrates how traditional inference tools can lead to invalid scientific conclusions, and previews the results of the post-selection inferential tools we develop in this article. Here, we use a 2-step WBS to estimate two locations $\widehat{b}_1$ and $\widehat{b}_2$ that segment the measured $\log_2$ ratios. Naively we might run t-tests for equality of means between the left and right neighboring segments of each estimated locations with the null hypothesis $H_0 : \boldsymbol{v}_j^T \boldsymbol{\theta} = 0$, for $j = 1, 2$ using the contrast vectors defined in (2). However, this would deem both changepoint locations as statistically significant, but an external karotyping dataset (from Snijders et al. (2001)) reveals that only one of the estimated locations is associated with a true CNV. At a high level, the t-test's erroneously small p-value arise since WBS detects specific changepoint locations because the empirical means to its left and right are well-separated, making the t-tests' null-hypotheses incorrect. To overcome this problem, we adapt the post-selection inference framework to the changepoint setting. As we will discuss in detail, our inferential tools can be done using either *saturated model* and a *selected model* on the mean vector $\boldsymbol{\theta}$. Moreover, using either such models leads to correctly deeming only one of the estimated changepoints as significant. We return to this dataset in Section 4.

[Figure 1 about here.]

We emphasize that while this motivating analysis is only for a single chromosome on one cell line, CNV analyses typically investigate the entire genome across many cell lines. Hence, an inflation in Type-I error can have profound effect in aggregate. Our inferential tools are well suited for these situations, as they can be used in an automated fashion as a way to filter out estimated changepoints in CNV analyses in a statistically-principled fashion.

1.2 *Related work*

The most common variant of post-selection inference is *sample splitting*, as discussed in Fithian et al. (2014). In our setting, this can be performed by dividing every odd and even index of $\boldsymbol{y}$ into two separate vectors, then applying BS or its variants on one vector, and using t-tests on the other. Since the data used to estimate the changepoints is independent of the data used for inference, this procedure yields valid p-values. However, as we will demonstrate empirically in Section 3, sample splitting reduces the test's power. Hence, in this article, we are interested in post-selection inferential tools that avoid sample splitting.

We mention additional works that use post-selection inference tools for changepoint detection. Most relevantly, Hyun et al. (2018) develop post-inference tools for the generalized lasso (a generalization of the fused lasso), which can also be used for inference in the changepoint setting as well. However, those tools do not directly work for the variants of BS considered in this article, and we additionally investigate methods to improve our tools' statistical power. Also, while writing this article, we became aware of the independent contributions in Duy et al. (2020), which appeared after the initial release of this article and develops variants that further improve our tools' statistical power. We remark that these notions of improved statistical power in this work is demonstrated mainly with empirical evidence. To the best of our knowledge, Azaïs et al. (2018) is the only article that proves the power of post-selection inference methods, but its theoretical setting is not applicable for most changepoint analyses we encounter in practice. Aside from these articles, there is little focus on valid post-detection

inference methods in changepoint analysis. On the other hand, there is a large literature on inference for *fixed* hypotheses in changepoint problems; we refer to works like Jandhyala et al. (2013).

2. Preliminaries

2.1 *Review: changepoint algorithms*

Below we describe the changepoint algorithms that we will study in this article. We will focus on formulations that run the algorithm for a given number of steps k. In what follows, we use the notation $\boldsymbol{y}_{a:b} = (y_a, y_{a+1}, \ldots, y_b)$ and $\overline{y}_{a:b} = (b-a+1)^{-1} \sum_{i=a}^{b} y_i$ for a vector $\boldsymbol{y}$. Similarly, for a set $\boldsymbol{I}$, $\overline{y}_I = |\boldsymbol{I}|^{-1} \sum_{i \in I} y_i$.

Binary segmentation (BS). Given a data vector $\boldsymbol{y} \in \mathbb{R}^n$, the k-step BS algorithm (see (Fryzlewicz, 2014) and refers within) sequentially splits the data based on the cumulative sum (CUSUM) statistics, defined below. At a step $\ell = 1, \ldots, k$, let $\widehat{\boldsymbol{b}}_{1:(\ell-1)}$ be the changepoints estimated so far, and let $\boldsymbol{I}_j$, $j = 1, \ldots, \ell$ be the partition of $\{1, \ldots, n\}$ induced by $\widehat{\boldsymbol{b}}_{1:(\ell-1)}$. Throughout this article, we use the convention that for $\ell = 1$, $\boldsymbol{I}_1 = \{1, \ldots, n\}$. Intervals of length 1 are discarded. Let s_j and e_j be the start and end indices of $\boldsymbol{I}_j$. The next changepoint $\widehat{b}_\ell$ and maximizing interval $\widehat{j}_\ell$ are chosen to maximize the absolute CUSUM statistic,

$$\{\widehat{j}_\ell, \widehat{b}_\ell\} = \underset{\substack{j \in \{1,\ldots,\ell-1\} \\ b \in \{s_j,\ldots,e_j-1\}}}{\operatorname{argmax}} \left| \boldsymbol{g}_{(s_j,b,e_j)}^T \boldsymbol{y} \right|, \quad \text{where} \quad \boldsymbol{g}_{(s,b,e)}^T \boldsymbol{y} = \sqrt{\frac{1}{\frac{1}{|e-b|} + \frac{1}{|b+1-s|}}} \left(\overline{y}_{(b+1):e} - \overline{y}_{s:b} \right). \quad (3)$$

Additionally, the direction $\widehat{d}_\ell$ of the new changepoint is calculated by the sign of the maximizing absolute CUSUM statistic, $\widehat{d}_\ell = \operatorname{sign}(\boldsymbol{g}_{(s_j,b_\ell,e_j)}^T \boldsymbol{y})$ for $j = \widehat{j}_{\ell+1}$.

Wild binary segmentation (WBS). The k-step WBS algorithm (Fryzlewicz, 2014) is a modification of BS that calculates CUSUM statistics over randomly drawn segments of the data. Denote by $\boldsymbol{w} = \{\boldsymbol{w}_1, \ldots, \boldsymbol{w}_B\} = \{(s_1, \ldots, e_1), \ldots, (s_B, \ldots, e_B)\}$ a set of B uniformly randomly drawn intervals with $1 \leqslant s_i < e_i \leqslant n$, $i = 1, \ldots, B$. At a step $\ell = 1, \ldots, k$, let J_ℓ to be the index set of the intervals in $\boldsymbol{w}$ which do not intersect with the changepoints $\widehat{\boldsymbol{b}}_{1:(\ell-1)}$

estimated so far. The next changepoint $\widehat{b}_\ell$ and the maximizing interval $\widehat{j}_\ell$ are obtained by

$$\{\widehat{j}_\ell, \widehat{b}_\ell\} = \underset{\substack{j \in J_\ell \\ b \in \{s_j, \ldots, e_j - 1\}}}{\operatorname{argmax}} \left| \boldsymbol{g}_{(s_j, b, e_j)}^T \boldsymbol{y} \right|,$$

where $\boldsymbol{g}_{(s,b,e)}^T \boldsymbol{y}$ is defined in (3). Similar to BS, the direction of the changepoint $\widehat{d}_\ell$ is defined by the sign of the maximizing absolute CUSUM statistic. Fryzlewicz (2014) shows that the theoretical guarantees for WBS is strictly better than that for BS. However, while both can estimate the true changepoints asymptotically in a theoretic sense, both are prone to mistakes with finite data. This necessitates the need to develop valid inferential tools to prune the estimated changepoints.

We also consider circular binary segmentation (CBS) and the comparisons to the fused lasso (FL) in this article, but defer their discussions to Appendix C for brevity.

2.2 *Review: post-selection inference*

We briefly review post-selection inference as developed in Fithian et al. (2014) and related work, adapted for changepoint problems. For clarity, we notationally distinguish between a random vector $\boldsymbol{Y}$ distributed as in (1), and $\boldsymbol{y}_{\text{obs}}$, a single data vector we observe for changepoint analysis. When a changepoint algorithm—such as BS, WBS, or CBS —is applied to the data $\boldsymbol{y}_{\text{obs}}$, it selects a particular changepoint model $M(\boldsymbol{y}_{\text{obs}})$. The specific forms of such models are described in Section 3.1; for now we may loosely think of $M(\boldsymbol{y}_{\text{obs}})$ as the changepoint locations and directions estimated by the algorithm on $\boldsymbol{y}_{\text{obs}}$, the data at hand. Post-selection inference revolves around the selective distribution, i.e., the law of

$$\boldsymbol{v}^T \boldsymbol{Y} \mid \Big(M(\boldsymbol{Y}) = M(\boldsymbol{y}_{\text{obs}}),\ q(\boldsymbol{Y}) = q(\boldsymbol{y}_{\text{obs}}) \Big), \tag{4}$$

under the null hypothesis $H_0 : \boldsymbol{v}^T \boldsymbol{\theta} = 0$, for any vector $\boldsymbol{v}$ that is a measurable function of $M(\boldsymbol{y}_{\text{obs}})$, such as in (2). Here, $q(\boldsymbol{Y})$ is a vector of sufficient statistic of nuisance parameters that need to be conditioned on in order to tractably compute inferences based on (4). The explicit form of $q(\boldsymbol{Y})$ differs based on the assumptions imposed on $\boldsymbol{\theta}$ under the null model.

Broadly, there are two classes of null models we may study: saturated and selected models (Fithian et al., 2014). As shown in the literature, computationally, in either null models, it is important for the selection event $\{\boldsymbol{y} : M(\boldsymbol{y}) = M(\boldsymbol{y}_{\text{obs}})\}$ be polyhedral. This is described in detail in Section 3.1, where we show that this holds for BS, WBS, and CBS.

Saturated model. The *saturated model* assumes that $\boldsymbol{Y}$ is distributed as in (1) with known error variance σ^2, and assumes nothing about the mean vector $\boldsymbol{\theta}$. We set $q(\boldsymbol{Y}) = \Pi_{\boldsymbol{v}}^{\perp}\boldsymbol{Y}$, the projection of $\boldsymbol{Y}$ onto the hyperplane orthogonal to $\boldsymbol{v}$. The selective distribution (4) then becomes the law of

$$\boldsymbol{v}^T\boldsymbol{Y} \mid \Big(M(\boldsymbol{Y}) = M(\boldsymbol{y}_{\text{obs}}),\ \Pi_{\boldsymbol{v}}^{\perp}\boldsymbol{Y} = \Pi_{\boldsymbol{v}}^{\perp}\boldsymbol{y}_{\text{obs}}\Big). \tag{5}$$

Selected model. The *selected model* again assumes that Y follows (1), but additionally assumes that the mean vector $\boldsymbol{\theta}$ is piecewise constant with changepoints at the sorted estimated locations $\widehat{\boldsymbol{c}}_{1:k} = \widehat{\boldsymbol{c}}_{1:k}(\boldsymbol{y}_{\text{obs}})$, assuming we have run our changepoint algorithm for k steps. That is, letting s_j and e_j denote the start and end index of interval I_j, we assume

$$\theta_{s_j} = \ldots = \theta_{e_j}, \quad j \in \{1, \ldots, k+1\}.$$

Under this assumption, the law of $\boldsymbol{Y}$ becomes a $(k+1)$-parameter Gaussian distribution. Additionally, with the contrast vector $\boldsymbol{v}_j$ defined as in (2), for any fixed $j = 1, \ldots, k+1$, the quantity $\boldsymbol{v}_j^T\boldsymbol{\theta}$ of interest is simply the difference between two of the parameters in this distribution. Specifically, let $\mathcal{I}_j = \{1, \ldots, k+1\}\backslash\{j, j+1\}$. Assuming σ^2 is known, the sufficient statistics $q(\boldsymbol{Y})$ are then the sample averages of the appropriate data segments, and the selective distribution (4) becomes the law of

$$\big(\overline{Y}_{\boldsymbol{I}_{j+1}} - \overline{Y}_{\boldsymbol{I}_j}\big) \mid \Big(M(\boldsymbol{Y}) = M(\boldsymbol{y}_{\text{obs}}),\ \overline{Y}_{\boldsymbol{I}_j \cup \boldsymbol{I}_{j+1}} = \big(\overline{y}_{\text{obs}}\big)_{\boldsymbol{I}_j \cup \boldsymbol{I}_{j+1}},\ \overline{Y}_{\boldsymbol{I}_\ell} = \big(\overline{y}_{\text{obs}}\big)_{\boldsymbol{I}_\ell} \text{ for } \ell \in \mathcal{I}_j\Big). \tag{6}$$

The appeal of the selected model is that we can properly treat σ^2 as unknown; in this case, we must only additionally condition on the Euclidean norm of y_{obs} to cover this nuisance

parameter, and the selective distribution (4) becomes the law of

$$\left(\overline{Y}_{\boldsymbol{I}_{j+1}} - \overline{Y}_{\boldsymbol{I}_j}\right) \,\Big|\, \Big(M(\boldsymbol{Y}) = M(\boldsymbol{y}_{\text{obs}}),\ \overline{Y}_{\boldsymbol{I}_j \cup \boldsymbol{I}_{j+1}} = \left(\overline{y}_{\text{obs}}\right)_{\boldsymbol{I}_j \cup \boldsymbol{I}_{j+1}},\ \overline{Y}_{\boldsymbol{I}_\ell} = \left(\overline{y}_{\text{obs}}\right)_{\boldsymbol{I}_\ell} \text{ for } \ell \in \mathcal{I}_j, \\ \|\boldsymbol{Y}\|_2 = \|\boldsymbol{y}_{\text{obs}}\|_2\Big). \quad (7)$$

3. Inference for changepoint algorithms

We describe our contributions that enable post-selection inference for changepoint analyses, beginning with the form of model selection events. We then describe computational details for saturated and selected model tests, and auxiliary randomization.

3.1 *Polyhedral selection events*

We show that, for each of the BS and WBS algorithms, there is a parametrization for their models such that event $\{\boldsymbol{y} : M(\boldsymbol{y}) = M(\boldsymbol{y}_{\text{obs}})\}$ is a polyhedron of the form $\{\boldsymbol{y} : \boldsymbol{\Gamma}\boldsymbol{y} \geqslant \boldsymbol{0}\}$, for a matrix $\boldsymbol{\Gamma} \in \mathbb{R}^{m \times n}$ that depends on $M(\boldsymbol{y}_{\text{obs}})$, where we interpret the inequality $\boldsymbol{\Gamma}\boldsymbol{y} \geqslant \boldsymbol{0}$ componentwise. Throughout the description of the polyhedra for each algorithm, we display the number of rows in $\boldsymbol{\Gamma}$ since it loosely denotes how "complex" each model selection event is. Overall, for a fixed k, the number of rows in $\boldsymbol{\Gamma}$ matrix for BS is linear in n, and $O(Bp)$ for WBS using intervals of length p. This number can grow faster than linear in n if $B \geqslant n$, which is recommended in practice (Fryzlewicz, 2014). All the proofs are provided in Appendix H.

Selection event for BS. We define the model for the k-step BS estimator as

$$M^{\text{BS}}_{1:k}(\boldsymbol{y}_{\text{obs}}) = \left\{\widehat{\boldsymbol{b}}_{1:k}(\boldsymbol{y}_{\text{obs}}),\ \widehat{\boldsymbol{d}}_{1:k}(\boldsymbol{y}_{\text{obs}})\right\},$$

where $\widehat{\boldsymbol{b}}_{1:k}(\boldsymbol{y}_{\text{obs}})$ and $\widehat{\boldsymbol{d}}_{1:k}(\boldsymbol{y}_{\text{obs}})$ are the changepoint locations and directions when the algorithm is run on $\boldsymbol{y}_{\text{obs}}$, as described in Section 2.1.

PROPOSITION 1: *Given any fixed $k \geqslant 1$ and $\boldsymbol{b}_{1:k}, \boldsymbol{d}_{1:k}$, we can explicitly construct $\boldsymbol{\Gamma}$ where*

$$\left\{\boldsymbol{y} : M^{\text{BS}}_{1:k}(\boldsymbol{y}) = \{\boldsymbol{b}_{1:k}, \boldsymbol{d}_{1:k}\}\right\} = \{\boldsymbol{y} : \boldsymbol{\Gamma}\boldsymbol{y} \geqslant \boldsymbol{0}\},$$

where $\boldsymbol{\Gamma}$ has $2\sum_{\ell=1}^{k}(n - \ell - 1)$ rows.

Selection event for WBS. We define the model of the k-step WBS estimator as

$$M^{\text{WBS}}_{1:k}(\boldsymbol{y}_{\text{obs}}, \boldsymbol{w}) = \big\{\widehat{\boldsymbol{b}}_{1:k}(\boldsymbol{y}_{\text{obs}}),\ \widehat{\boldsymbol{d}}_{1:k}(\boldsymbol{y}_{\text{obs}}),\ \widehat{\boldsymbol{j}}_{1:k}(\boldsymbol{y}_{\text{obs}})\big\},$$

where $\boldsymbol{w}$ is the set of B intervals that the algorithm uses, $\widehat{\boldsymbol{b}}_{1:k}(\boldsymbol{y}_{\text{obs}})$ and $\widehat{\boldsymbol{d}}_{1:k}(\boldsymbol{y}_{\text{obs}})$ are the changepoint locations and directions, and $\widehat{\boldsymbol{j}}_{1:k}(\boldsymbol{y}_{\text{obs}})$ are the maximizing intervals. Note that unlike BS, the maximizing intervals $\widehat{\boldsymbol{j}}_{1:k}$ are part of WBS's model.

PROPOSITION 2: *Given any fixed $k \geqslant 1$ and $\{\boldsymbol{w}, \boldsymbol{b}_{1:k}, \boldsymbol{d}_{1:k}, j_{1:k}\}$, we can explicitly construct $\boldsymbol{\Gamma}$ where*

$$\big\{\boldsymbol{y} : M^{\text{WBS}}_{1:k}(\boldsymbol{y}, \boldsymbol{w}) = \{\boldsymbol{b}_{1:k}, \boldsymbol{d}_{1:k}, \boldsymbol{j}_{1:k}\}\big\} = \big\{\boldsymbol{y} : \boldsymbol{\Gamma}\boldsymbol{y} \geqslant \boldsymbol{0}\big\}.$$

The number of rows in $\boldsymbol{\Gamma}$ will vary depending on the configuration of w and $b_{1:k}$, but if each of the B intervals in w has length p, it will be at most $2\sum_{\ell=1}^{k}((B-\ell)\cdot(p-1)+(p-2))$.

In Appendix C, we additionally state the analogous results for the CBS model, as well as review the results for the FL model as derived in Hyun et al. (2018) for comparison.

3.2 *Computation of p-values*

Given a precise description of the polyhedral selection event $\{\boldsymbol{y} : M(\boldsymbol{y}) = M(\boldsymbol{y}_{\text{obs}})\}$, we can describe the methods to compute the p-value, i.e. the tail probability of the selective distributions described in Section 2.2. Without loss of generality, all of our descriptions will be specialized to testing the null hypothesis of $H_0 : \boldsymbol{v}^T\boldsymbol{\theta} = 0$ against the one-sided alternative $H_1 : \boldsymbol{v}^T\boldsymbol{\theta} > 0$. For saturated model tests, this exact calculation has been developed in previous works and we review it as it is relevant to our contributions on increasing its power. For selected model tests, we develop a new hit-and-run sampler. We emphasize, as stated in works like Fithian et al. (2014), the following methods provide p-values that are *exactly* uniformly distributed under the null hypothesis with respect to n, unlike those from t-tests.

Saturated model tests: exact formulae. As shown in Tibshirani et al. (2018) and related work, the saturated selective distribution (5) has a particularly computationally

convenient distribution when $\boldsymbol{Y}$ is Gaussian and the model selection event $\{\boldsymbol{y} : M(\boldsymbol{y}) = M(\boldsymbol{y}_{\text{obs}})\}$ is a polyhedral set in $\boldsymbol{y}$. In this case, the law of (5) is a *truncated Gaussian* (TG), whose truncation limits depend only on $\Pi_{\boldsymbol{v}}^{\perp}\boldsymbol{y}_{\text{obs}}$, and can be computed explicitly. Its tail probability can be computed in closed form (without Monte Carlo sampling). That is, the probability that $\boldsymbol{v}^T\boldsymbol{Y} \geqslant \boldsymbol{v}^T\boldsymbol{y}_{\text{obs}}$ under the law of (5) is exactly equal to

$$\big\{\Phi(\mathcal{V}_{\text{up}}/\tau) - \Phi(\boldsymbol{v}^T\boldsymbol{y}_{\text{obs}}/\tau)\big\}/\big\{\Phi(\mathcal{V}_{\text{up}}/\tau) - \Phi(\mathcal{V}_{\text{lo}}/\tau)\big\} \tag{8}$$

where $\Phi(\cdot)$ represents the standard Gaussian CDF, $\tau = \sigma^2\|\boldsymbol{v}\|_2^2$, $\boldsymbol{\rho} = \boldsymbol{\Gamma}\boldsymbol{v}/\|\boldsymbol{v}\|_2^2$ and

$$\mathcal{V}_{\text{lo}} = \boldsymbol{v}^T\boldsymbol{y}_{\text{obs}} - \min_{j:\rho_j>0}\big(\boldsymbol{\Gamma}\boldsymbol{y}_{\text{obs}}\big)_j/\rho_j, \quad \text{and} \quad \mathcal{V}_{\text{up}} = \boldsymbol{v}^T\boldsymbol{y}_{\text{obs}} - \max_{j:\rho_j<0}\big(\boldsymbol{\Gamma}\boldsymbol{y}_{\text{obs}}\big)_j/\rho_j. \tag{9}$$

The statistic in (8) is commonly referred as the TG statistic. Since this statistic is a pivot and lies between $[0, 1]$, it is the p-value used for the saturated model test.

Selected model tests: hit-and-run sampling. To compute the p-value for selected model tests, Fithian et al. (2015) proposed a hit-and-run strategy for sampling from the distribution for the known σ^2 setting, (6). This was implemented by the authors, and we briefly review the details in Appendix D. For the unknown σ^2 setting, Fithian et al. (2014) developed an importance sampling strategy for sampling the distribution (7). However, we develop an alternative and intuitive hit-and-run strategy can be adapted to the unknown σ^2 setting and implement this as a new algorithm.

Given a changepoint $j \in \{1, \ldots, k\}$, observe that we can design a segment test contrast $\boldsymbol{v}$ where sampling from (7) is equivalent to sampling uniformly from the set

$$\Big\{\boldsymbol{v}^T\boldsymbol{Y} : M(\boldsymbol{Y}) = M(\boldsymbol{y}_{\text{obs}}),\ \|\boldsymbol{Y}\|_2 = \|\boldsymbol{y}_{\text{obs}}\|_2,\ \overline{Y}_{\boldsymbol{I}_j\cup\boldsymbol{I}_{j+1}} = \big(\overline{y}_{\text{obs}}\big)_{\boldsymbol{I}_j\cup\boldsymbol{I}_{j+1}},\ \overline{Y}_{\boldsymbol{I}_\ell} = \big(\overline{y}_{\text{obs}}\big)_{\boldsymbol{I}_\ell} \text{ for } \ell \in \mathcal{I}_j\Big\}. \tag{10}$$

Note that the above set no longer depends on $\boldsymbol{\theta}$ or σ^2. This is because we conditioned all the relevant sufficient statistics under the selected model. Our hit-and-run sampler then sequentially draws samples $\boldsymbol{v}^T\boldsymbol{Y}$ from the above set. For brevity, the explicit algorithm

is deferred to Appendix D, and leverages explicit formulas computing the intersection of 2-dimensional circles with polytopes.

3.3 *Randomization and marginalization*

We apply the ideas of auxiliary randomization in Tian and Taylor (2018) to improve the power of post-selection inference for changepoint algorithms. We investigate two specific forms of randomization – randomization over additive noise or over random intervals – specialized for satured models. We note that similar randomization of selected model inferences is also possible but is doubly computationally burdensome.

Marginalization over additive noise. Tian and Taylor (2018) shows that performing inference based on the selected model $M(\boldsymbol{y}_{\text{obs}} + \boldsymbol{w}_{\text{obs}})$ where $\boldsymbol{w}_{\text{obs}}$ is additive noise and then marginalizing over $\boldsymbol{W}$ leads to improved power. Here, $\boldsymbol{w}_{\text{obs}}$ is a realization of a random component $\boldsymbol{W}$ sampled from $\mathcal{N}(\boldsymbol{0}, \sigma^2_{\text{add}}\boldsymbol{I}_n)$, where $\sigma^2_{\text{add}} > 0$ is set by the user. Fithian et al. (2014) provides a mathematical framework for pursuing such randomization, stating that less conditioning results in an increase in Fisher information. For additive noise, the above model selection event is:

$$\{\boldsymbol{y} : \boldsymbol{\Gamma}(\boldsymbol{y} + \boldsymbol{w}_{\text{obs}}) \geqslant \boldsymbol{0}\} = \{\boldsymbol{y} : \boldsymbol{\Gamma}\boldsymbol{y} \geqslant -\boldsymbol{\Gamma}\boldsymbol{w}_{\text{obs}}\}.$$

This suggests the following idea of using existing machinery to formulate the polyhedron formed by the model selection event based on perturbed data $\boldsymbol{y}_{\text{obs}} + \boldsymbol{w}_{\text{obs}}$.

Porting the ideas of Tian and Taylor (2018) to our setting, to test the one-sided null hypothesis $H_0 : \boldsymbol{v}^T\boldsymbol{\theta} = 0$, we want to compute the following tail probability of the marginalized selective distribution,

$$T(\boldsymbol{y}_{\text{obs}}, \boldsymbol{v}) = \mathbb{P}\Big(\boldsymbol{v}^T\boldsymbol{Y} \geqslant \boldsymbol{v}^T\boldsymbol{y}_{\text{obs}} \;\Big|\; \Big(M(\boldsymbol{Y} + \boldsymbol{W}) = M(\boldsymbol{y}_{\text{obs}} + \boldsymbol{W}),\ \Pi^{\perp}_{\boldsymbol{v}}\boldsymbol{Y} = \Pi^{\perp}_{\boldsymbol{v}}\boldsymbol{y}_{\text{obs}}\Big)\Big). \quad (11)$$

It is hard to directly compute this. However, the formulas in (8) and (9) give us exact

formulas to compute the non-marginalized tail-probabilities,

$$T(\boldsymbol{y}_{\text{obs}}, \boldsymbol{v}, \boldsymbol{w}_{\text{obs}}) = \mathbb{P}\Big(\boldsymbol{v}^T\boldsymbol{Y} \geqslant \boldsymbol{v}^T\boldsymbol{y}_{\text{obs}} \;\Big|\; \Big(M(\boldsymbol{Y}+\boldsymbol{W}) = M(\boldsymbol{y}_{\text{obs}}+\boldsymbol{W}),\ \Pi_{\boldsymbol{v}}^{\perp}\boldsymbol{Y} = \Pi_{\boldsymbol{v}}^{\perp}\boldsymbol{y}_{\text{obs}},\ \boldsymbol{W} = \boldsymbol{w}_{\text{obs}}\Big)\Big).$$

The following proposition shows that we can compute $T(\boldsymbol{y}_{\text{obs}}, \boldsymbol{v})$ by reweighting instances of $T(\boldsymbol{y}_{\text{obs}}, \boldsymbol{v}, \boldsymbol{w}_{\text{obs}})$ via importance sampling. Here, let $E_1 = \mathbb{1}[M(\boldsymbol{Y} + \boldsymbol{W}) = M(\boldsymbol{y}_{\text{obs}} + \boldsymbol{W})]$ and $E_2 = \mathbb{1}[\Pi_{\boldsymbol{v}}^{\perp}\boldsymbol{Y} = \Pi_{\boldsymbol{v}}^{\perp}\boldsymbol{y}_{\text{obs}}]$.

PROPOSITION 3: *Let Ω denote the support of the random component $\boldsymbol{W}$. If the distribution of $\boldsymbol{W}$ is independent of the random event E_2, (11) can be exactly computed as*

$$T(\boldsymbol{y}_{\text{obs}}, \boldsymbol{v}) = \int_{\Omega} T(\boldsymbol{y}_{\text{obs}}, \boldsymbol{v}, \boldsymbol{w}_{\text{obs}}) \cdot a(\boldsymbol{w}_{\text{obs}})\, dP_{\boldsymbol{W}}(\boldsymbol{w}_{\text{obs}}) = \frac{\int_{\Omega} \Phi\big(\mathcal{V}_{up}/\tau\big) - \Phi\big(\boldsymbol{v}^T\boldsymbol{y}_{\text{obs}}/\tau\big)\, dP_{\boldsymbol{W}}(\boldsymbol{w}_{\text{obs}})}{\int_{\Omega} \Phi\big(\mathcal{V}_{up}/\tau\big) - \Phi\big(\mathcal{V}_{lo}/\tau\big)\, dP_{\boldsymbol{W}}(\boldsymbol{w}_{\text{obs}})}. \tag{12}$$

where the weighting factor is $a(\boldsymbol{w}_{\text{obs}}) = \mathbb{P}(\boldsymbol{W} = \boldsymbol{w}_{\text{obs}}|E_1, E_2)/\mathbb{P}(\boldsymbol{W} = \boldsymbol{w}_{\text{obs}})$.

The first equality in (12) demonstrates the reweighting of $T(\boldsymbol{y}_{\text{obs}}, \boldsymbol{v}, \boldsymbol{w}_{\text{obs}})$, but the second equality gives a sampling strategy where we approximate the integrals. Specifically, we sample T different instances of $\boldsymbol{w}_{\text{obs}}$ and compute $k(\boldsymbol{w}_{\text{obs}})$ and $g(\boldsymbol{w}_{\text{obs}})$, denoting the integrand of the last term's numerator and denominator in (12) respectively. Then the approximate for the tail probability (12) is the ratio between the summation of all the instances of $k(\boldsymbol{w}_{\text{obs}})$ and of all instances of $g(\boldsymbol{w}_{\text{obs}})$. (Observe that the calculations of $\mathcal{V}_{\text{up}}$ and $\mathcal{V}_{\text{lo}}$ now involve $\boldsymbol{w}_{\text{obs}}$.) For brevity, we defer the explicit algorithm to Appendix D.

Marginalization over WBS intervals. In contrast to the above setting where $\boldsymbol{W}$ represents Gaussian noise, in WBS described in Section 2.1, W represents the set of B randomly drawn intervals. Observe that Proposition 3 still applies to this setting, where $M(\boldsymbol{y}_{\text{obs}} + \boldsymbol{w}_{\text{obs}})$ is now replaced with $M(\boldsymbol{y}_{\text{obs}}, \boldsymbol{w}_{\text{obs}})$, as described in Section 3.1. However, unlike the additive noise setting, the maximizing intervals $\widehat{\boldsymbol{j}}_{1:k}$ in the model $M(\boldsymbol{y}_{\text{obs}}, \boldsymbol{w}_{\text{obs}})$ are embedded in the construction of the matrix $\boldsymbol{\Gamma}$ representing the polyhedra. This prevents a naive sampling of B new intervals. To overcome this, let $\{\boldsymbol{W}_{\widehat{j}_1}, \ldots, \boldsymbol{W}_{\widehat{j}_k}\}$ be the maximizing

intervals. We sample a new set of all other intervals, W_ℓ for $\ell \in \{1, \ldots, B\} \backslash \{\widehat{j}_1, \ldots, \widehat{j}_k\}$. Specifically, for each of such intervals $\boldsymbol{W}_\ell = (s_\ell, \ldots, e_\ell)$, the indices s_ℓ and e_ℓ are sampled uniformly between 1 to n where $s_\ell < e_\ell$. After all $B - k$ intervals are resampled, a check is performed to ensure that $\{\boldsymbol{W}_{\widehat{j}_1}, \ldots, \boldsymbol{W}_{\widehat{j}_k}\}$ are still the maximizing intervals when WBS is applied again to $\boldsymbol{y}_{\text{obs}}$. The full algorithm is also deferred to Appendix D.

3.4 *Simulation results*

We provide a brief overview of simulation-based results that demonstrate the utility of our inferential tools, highlighting that our selected model tests and marginalized saturated model tests empirically higher power than plain saturated model tests and t-tests based on sample splitting, described in Section 1.2. In these simulations, we generate Gaussian data with $\boldsymbol{\theta}$ having two changepoints with varying signal sizes, and try different testing procedures based on 2-step BS. We then compute the unconditional power of each test, defined as how often a test successfully detects the location of the true changepoint and then successfully rejects the null hypothesis. We make two observations from our results (Figure 2). First, the marginalized saturated model tests have substantially higher power over their plain counterparts, verifying the theoretical intuitions in Tian and Taylor (2018). Second, sample splitting leads to a lower unconditional power compared to our inferential tools primarily because sample splitting uses only half the data to detect changepoints, leading to a lower detection probability. Another competing method are the post-selection inference tools developed in Hyun et al. (2018). For brevity, we defer extensive simulations showing uniform null p-values, and those comparing the power among these methods, as well as additional details and discussions, to Appendix E.

[Figure 2 about here.]

4. Copy Number Variation (CNV) application

In this section, we apply our post-selection inference tools to study their empirical performance on both the aCGH data from Snijders et al. (2001) (introduced in Section 1) as well as sequencing data from Botton et al. (2013). Both datasets are specifically chosen since there are scientifically meaningful ways to quantify whether or not our inference tools were successful. Specifically, we first demonstrate in Section 4.1 that our inferential tools can be used for filtering changepoints by comparing our results applied on the aCGH data to external karotyping results. Then in Section 4.2, we show that we can adapt our inferential tools to handle heavy-tailed noise appearing in CNV analyses by demonstrating that p-values under the null hypothesis based on pseudo-real datasets are correctly distributed as uniform. Finally in Section 4.3, we show that while sequencing data (a newer technology based on counting DNA fragments) has technical variability that can differ dramatically from aCGH data (an older technology based on measuring light intensities), by preprocessing the sequencing data appropriately, our inferential tools shown to work for aCGH data can yield similar results on sequencing data. Together, these empirical results demonstrate that our inferential tools can be reliably used for automated filtering of changepoints for CNV analyses.

4.1 *Analysis on Snijders dataset*

We first extend our analysis of the Snijders dataset from Section 1 by detecting and inferring about CNVs across the entire genome of different cell lines. These datasets are ideal because a ground truth – external karotyping results – exists from the original study, which we compare our inferential results against. These cell lines originate from fibroblast cells and contain over $2,000$ probe measurements across all 23 chromosomes.

In our analysis, we use a 4-step WBS and perform marginalized saturated model tests across the genome on each of the four cell lines (GM02948, GM05296, GM01524, and GM01750), shown in Figure 3. We pre-cut at chromosome boundaries since the ordering of chromosomes

1 through 23 is essentially arbitrary, meaning we initialize WBS with changepoints at the boundaries between chromosomes, but do not consider these as estimated changepoints. We test at a significance level $\alpha = 0.05$ after Bonferroni correction. This is described in Appendix B. We provide additional details of our analyses in Appendix G.

Our results, shown in Figure 3, demonstrate that while WBS estimates changepoints at various locations across the genome, the significant changepoints determined by our inferential tools largely agree with external karotyping results. For example, in GM02948, external karotyping results show there is no CNV that occurs within a chromosome, and likewise, our inferential results filtered out all 4 estimated changepoints. Likewise, in GM05296 and GM01750, external karotyping match exactly with which changepoints were deemed as significant, and the remaining changepoints were filtered out. In GM01524 however, external karotyping results only validates the changepoints we estimated at chromosome 6. The analysis on these four cell lines demonstrates that our inferential tools can be used effectively to filter the changepoints across a wide range of scenarios.

[Figure 3 about here.]

4.2 *Follow-up analysis on Snijders dataset for impact of heavy tails*

While our inferential tools are designed for Gaussian data, we demonstrate that they can be adapted to handle heavy-tailed data by bootstrapping the residuals instead of explicitly calculating the tail probabilities. For example, we can observe the heavy-tailed nature in the Snijders dataset by focusing on chromosome 9 in GM01750 (Figure 4). A QQ plot of the residuals $\boldsymbol{r}$ (computed by taking the difference between the observation and the mean of its corresponding segment) suggests that the noise has heavier tails than a Gaussian (Figure 4A), and are closer in distribution to a Laplacian. Hence, we design a study based on pseduo-real datasets with heavy tails derived from this chromosome to investigate whether or not we can obtain uniform p-values under the null hypothesis in this setting.

To design this numerical study, we use the following procedure to generate pseudo-real datasets. Using the model $\boldsymbol{y} = \boldsymbol{\theta} + \boldsymbol{\epsilon}$, we add the noise variable ϵ in three different ways:

(1) Gaussian noise $\boldsymbol{\epsilon} \sim \mathcal{N}(\mathbf{0}, \sigma^2 \boldsymbol{I}_n)$,

(2) Laplace noise $\boldsymbol{\epsilon} \sim \text{Laplace}(\mathbf{0}, \sigma/\sqrt{2} \cdot \boldsymbol{I}_n)$, and

(3) Bootstrapped residuals, $\boldsymbol{\epsilon} = b(\boldsymbol{r})$, where $b(\cdot)$ samples the residuals $\boldsymbol{r}$ with replacement.

To simplify this study, we focus on the behavior of plain saturated model tests after a 3-step BS across all three types of noises under the null hypothesis $H_0 : \boldsymbol{v}^T\boldsymbol{\theta} = 0$.

[Figure 4 about here.]

The empirical distribution of the p-values under the null hypothesis under the three different noise models are shown in Figure 4B. Specifically, while the plain saturated model test yield valid Type-I error control under Gaussian noise, its Type-I error control under Laplacian noise and bootstrapped residuals is slightly inflated. We introduce the following variant of our inferential tools to resolve this inflation.

Our variant is a modification of the *bootstrap substitution method* originally proposed in Tibshirani et al. (2018). Here, we approximate the law of $\boldsymbol{v}^T\boldsymbol{Y}$ used to construct the TG statistic (8) with the bootstrapped distribution of $\boldsymbol{v}^T(\boldsymbol{Y} - \boldsymbol{\theta})$. Specifically, we consider bootstrapping the residuals, $\boldsymbol{r} = \boldsymbol{y} - \widehat{\boldsymbol{\theta}}$, where $\widehat{\boldsymbol{\theta}}$ is a piecewise constant estimate of $\boldsymbol{\theta}$. Here, we use a k-step BS model to estimate $\widehat{\boldsymbol{\theta}}$, where we choose k using 2-fold cross validation from a two-fold split of the data $\boldsymbol{y}$ into odd and even indices. For our dataset, while this procedure is not valid in general and should be used with caution, these potential downsides do not seem to come to fruition in practice. Importantly, for our analysis derived from chromosome 9 in GM01750, the resulting p-values using this bootstrapped variant under any of the three noise models are convincingly uniform (Figure 4D). We provide results in Appendix G.

4.3 *Analysis on Botton dataset*

While the above analysis were focused on aCGH data, we now show that our inferential tools can also be used in sequencing data used to study CNV if appropriately preprocessed. This is important to verify, as the technical noise of sequencing data without suitable preprocessing is vastly different from the technical noise of microarray data. Specifically, we investigate our inferential tools' performance on sequencing data collected in Botton et al. (2013) which was preprocessed using CNVkit (Talevich et al., 2016), a recent codebase designed to analyze CNV from sequencing data. This sequencing data is derived from the C0902 melanoma cell line, and has over 27,000 measurements across the entire genome. We choose this dataset in particular since we also have an external aCGH dataset of the same cell line, with comparable locations along the genome. Hence, we can see whether or not our inferential tools behave similarly between sequencing and aCGH data. We defer our preprocessing details performed by CNVkit to Appendix G.

The results, shown in Figure 5, demonstrates that while the estimated changepoints based on aCGH or sequencing data can differ dramatically, the significant changepoints determined by our inferential tools are largely the same. Specifically, we focus on chromosomes 5 and 10, and apply a 5-step WBS followed by marginalized saturated model tests. In chromosome 5, the changepoint around location 0.25 is deemed significant in both aCGH and sequencing data, and many of the other estimated changepoints that disagree between both data sources are filtered out. In chromosome 10, the changepoints around location 0.3 is deemed significant in both aCGH and sequencing data, and in this case, Talevich et al. (2016) perform FISH experiments that additionally reveal there is a true CNV at this location. Overall, we note that since these two data sources are different, we should not expect the significant changepoints to exactly match in general. However, as we have demonstrated, our inferential tools filter changepoints in a way that is largely stable across multiple data sources.

[Figure 5 about here.]

5. Conclusion

In this article, we have developed methods to perform valid post-selection inference for changepoint algorithms and applied them to CNV analyses. Through simulations, we have shown our inferential tools have higher power than competing methods. Through our applications on aCGH and sequencing data, we have shown that our inferential tools are beneficial for filtering changepoints. However, changepoint detection is a rapidly-evolving field, and this article provides a blueprint on how to perform post-selection inference for newer methods.

Acknowledgements

The authors used Pittsburgh Supercomputing Center resources (Proposal/Grant Number: DMS180016P). Sangwon Hyun was supported by supported by NSF grants DMS-1554123 and DMS-1613202. Max G'Sell was supported by NSF grant DMS-1613202. Ryan Tibshirani was supported by NSF grant DMS-1554123. We also thank Nancy R. Zhang for helpful discussions and suggestions.

References

Azaïs, J.-M., De Castro, Y., and Mourareau, S. (2018). Power of the spacing test for least-angle regression. *Bernoulli* **24,** 465–492.

Botton, T., Yeh, I., Nelson, T., Vemula, S. S., Sparatta, A., Garrido, M. C., Allegra, M., Rocchi, S., Bahadoran, P., McCalmont, T. H., et al. (2013). Recurrent BRAF kinase fusions in melanocytic tumors offer an opportunity for targeted therapy. *Pigment cell & melanoma research* **26,** 845–851.

Duy, V. N. L., Toda, H., Sugiyama, R., and Takeuchi, I. (2020). Computing valid p-value for

optimal changepoint by selective inference using dynamic programming. *arXiv preprint arXiv:2002.09132* .

Fithian, W., Sun, D., and Taylor, J. (2014). Optimal inference after model selection. arXiv: 1410.2597.

Fithian, W., Taylor, J., Tibshirani, R., and Tibshirani, R. J. (2015). Selective sequential model selection. arXiv: 1512.02565.

Fryzlewicz, P. (2014). Wild binary segmentation for multiple change-point detection. *Annals of Statistics* **42,** 2243–2281.

Hyun, S., G'Sell, M., and Tibshirani, R. J. (2018). Exact post-selection inference for the generalized lasso path. *Electronic Journal of Statistics* pages 1053–1097.

Jandhyala, V., Fotopoulos, S., Macneill, I., and Liu, P. (2013). Inference for single and multiple change-points in time series. *Journal of Time Series Analysis* **34,** 423–446.

Lin, K., Sharpnack, J. L., Rinaldo, A., and Tibshirani, R. J. (2017). A sharp error analysis for the fused lasso, with application to approximate changepoint screening. In *Advances in Neural Information Processing Systems*, pages 6884–6893.

Olshen, A., Seshan, V. E., Lucito, R., and Wigler, M. (2004). Circular binary segmentation for the analysis of array-based DNA copy number data. *Biostatistics* **5,** 557–572.

Snijders, A. M., Nowak, N., Segraves, R., Blackwood, S., Brown, N., Conroy, J., Hamilton, G., Hindle, A. K., Huey, B., Kimura, K., et al. (2001). Assembly of microarrays for genome-wide measurement of DNA copy number. *Nature genetics* **29,** 263–264.

Talevich, E., Shain, A. H., Botton, T., and Bastian, B. C. (2016). CNVkit: Genome-wide copy number detection and visualization from targeted DNA sequencing. *PLoS computational biology* **12,**.

Tian, X. and Taylor, J. (2018). Selective inference with a randomized response. *Annals of Statistics* **46,** 619–710.

Tibshirani, R. J., Rinaldo, A., Tibshirani, R., and Wasserman, L. (2018). Uniform asymptotic inference and the bootstrap after model selection. *Ann. Statist.* **46,** 1255–1287.

Zhang, N. R. (2010). DNA copy number profiling in normal and tumor genomes. In *Frontiers in Computational and Systems Biology*, pages 259–281. Springer.

Supporting information

Web Appendices, Tables, and Figures 6-14 referenced in Sections 1-5 are available with this paper at the Biometrics website on Wiley Online Library.

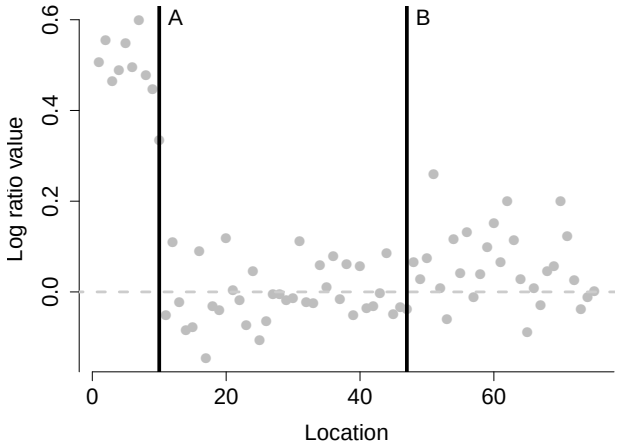

Location	A	B
Karyotype	True	False
Classical t-test	0	5×10^{-4}
Saturated model test	0	0.050
Selected model test	0	0.027

Figure 1: *(Left): aCGH data from the 14th chromosome of fibroblast cell line GM01750, from Snijders et al. (2001). The x-axis denotes the relative index of the genome position, and the y-axis denotes the measured* $\log_2$ *copy number ratio after a suitable preprocessing, with a dotted line denoting 0 for reference. The bold vertical lines denote the locations A and B from running WBS for 2 steps (corresponding to* $\widehat{b}_1$ *and* $\widehat{b}_2$*). (Right): The p-values using classical (naive) t-tests, saturated model tests, and selected model tests, at each location A and B. The ground truth is also given, as determined by karyotyping. The saturated model test used an estimated noise level* σ^2 *from the entire 23-chromosome data set. The selected model test was performed in the unknown* σ^2 *setting. Specifically, we test the null hypothesis* $H_0 : \boldsymbol{v}_j^T \boldsymbol{\theta} = 0$*, for* $j = 1, 2$*, where the contrast vectors are as defined in (2). We see that both saturated and selected model tests correcting determine only location A to be associated with a true CNV. Note: this figure appears in color in the electronic version of this article, and any mention of color refers to that version.*

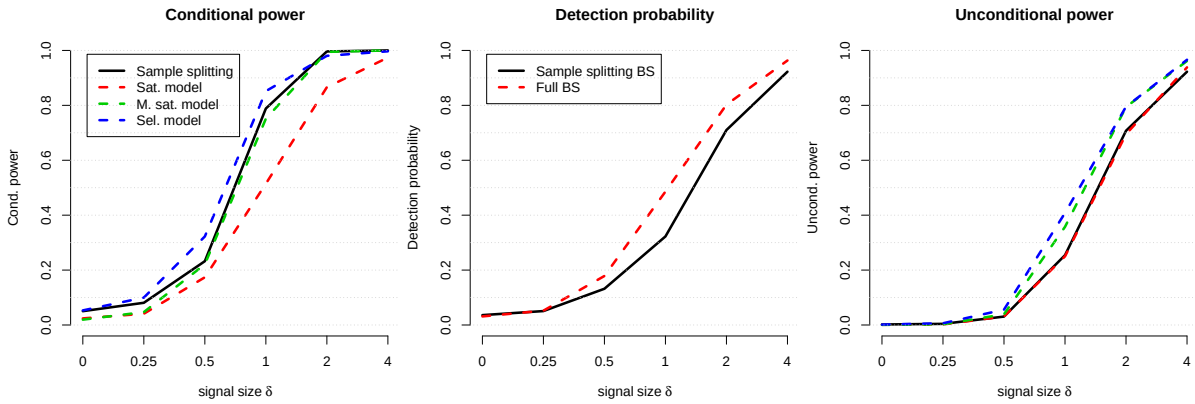

Figure 2: *Simulation results displaying the empirical power for plain saturated model test (red dashed), additive noise marginalized saturated model test (green dashed), and selected model test with unknown σ^2 (blue dashed), and t-test for equality of mean after sample splitting (black solid), performed after a 2-step BS. Here, we generate Gaussian data where $\boldsymbol{\theta}$ has two true changepoints, and δ (the x-axis) parameterizes the signal (i.e., the difference between the piecewise constant segments). A larger δ means an easier simulation setting. We try more than 250 trials for at each value of δ. (Left): Conditional power across all four methods, defined as the number of correctly detected and rejected changepoints instances divided by the number of corrected detected changepoints. (Middle): Detection probability for the BS, defined as the number of corrected detected changepoints divided by total number of trials. (Right): Unconditional power, defined by multiplying the conditional power curve and its relevant detection probability curve. Together, we see selected model tests and marginalized saturated model tests have higher unconditional power for larger δ than sample splitting and plain saturated model tests. More details behind the simulation are given in Appendix E. Note: this figure appears in color in the electronic version of this article, and any mention of color refers to that version. Note: this figure appears in color in the electronic version of this article, and any mention of color refers to that version.*

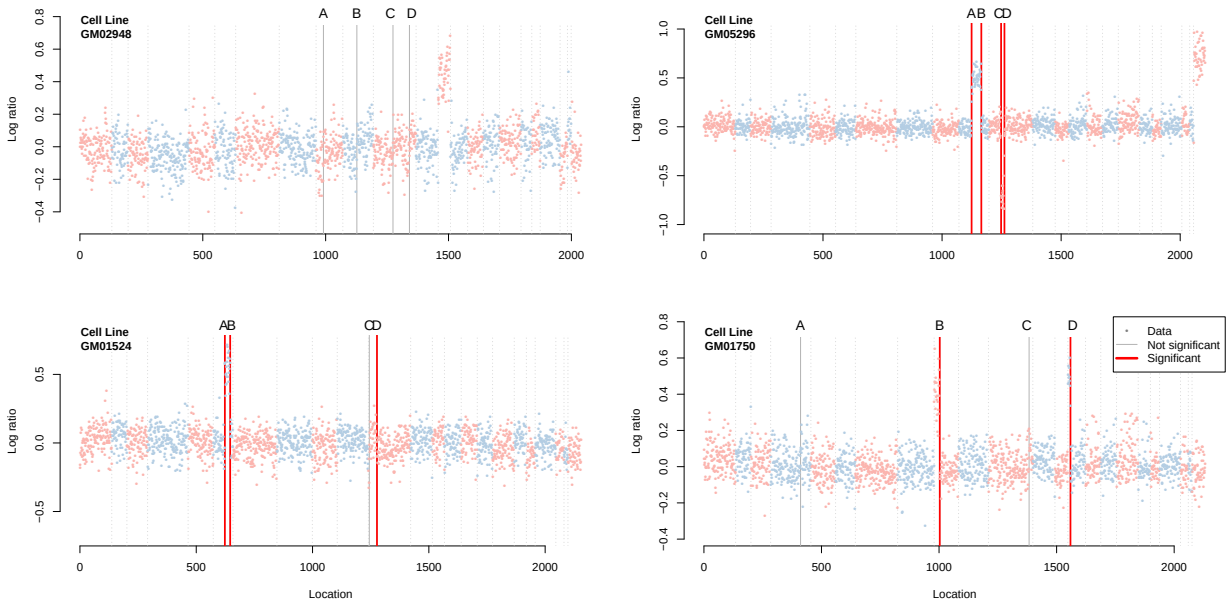

Figure 3: *Pre-cut changepoint inference using saturated model tests for 4-step WBS marginalized over random intervals conducted on four cell lines across all 23 chromosomes, from Snijders et al. (2001). Data points are colored in two alternating tones, to visually depict the chromosomal boundaries. The x-axis denotes the relative index of the genome position while the y-axis denotes the measured* $\log_2$ *copy number. For each cell line, the letters A through D denote the estimated changepoints,* $\widehat{c}_1$ *through* $\widehat{c}_4$ *respectively. The bolded gray (or red) horizontal lines denote changepoints that were rejected (or not rejected) under the null hypothesis* $H_0 : \boldsymbol{v}^T\boldsymbol{\theta} = 0$ *at a Type-I error control level* $\alpha = 0.05$ *after Bonferroni-correction. (Top left): The analysis for the cell line GM02948 with no significant changepoints. This matches external karotyping results, marking a trisomy (i.e., increase in copy number) of the entire chromosome 13, meaning there are no CNVs within any chromosome. (Top right): The analysis for the cell line GM05296 with 4 significant changepoints, all at chromosome 10 and 11. This matches external karotyping results, marking a trisomy al chromosome 10 and a monosomy (i.e., decrease in copy number) at chromosome 11. (Bottom left): The analysis for the cell line GM01524 with 3 significant changepoints, at chromosome 6 and 9. The external karotyping results only reveal that the CNV at chromosome 6 is true (i.e., 6q15 to 6q25). (Bottom right): The analysis for the cell line GM01750 with 2 significant changepoints, at chromosome 9 and 14. This matches external karotyping results, marking trisomies at chromosome 9 and 14. Note: this figure appears in color in the electronic version of this article, and any mention of color refers to that version.*

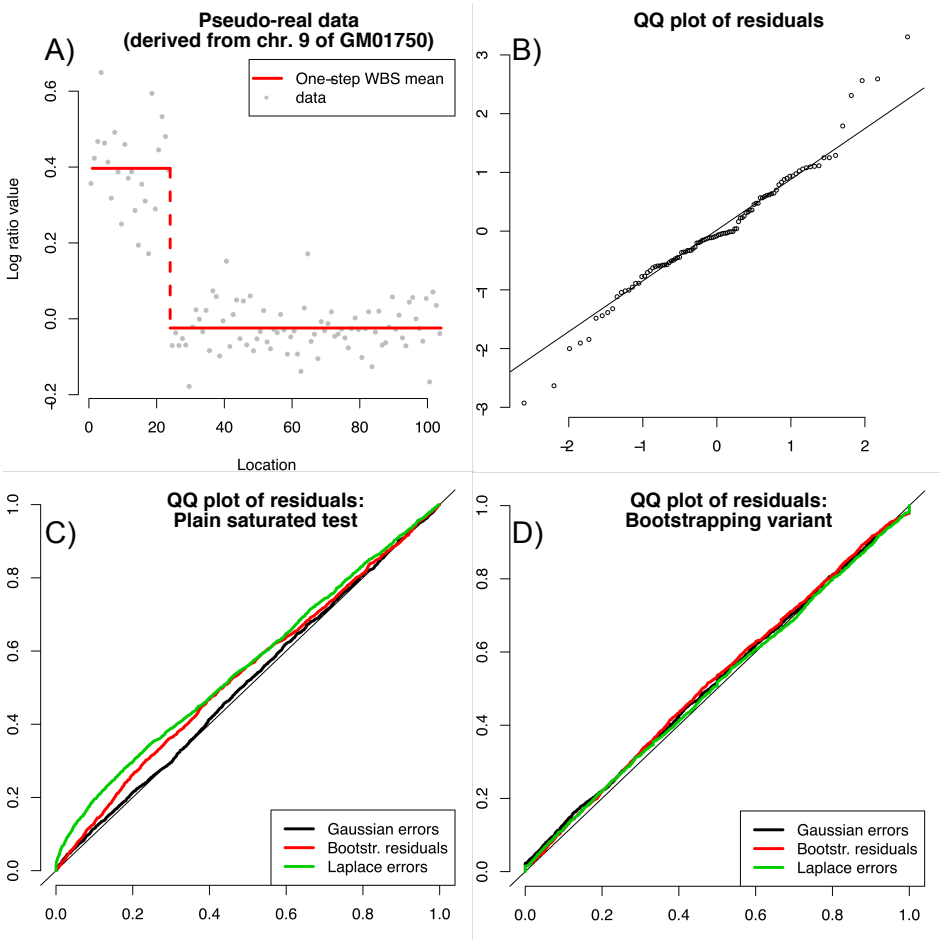

Figure 4: *(A) Bootstrapped residuals added to the artificially constructed mean, generated from chromosome 9 in GM01750. (B): QQ plot of residuals. The remaining 3 panels show the p-values of saturated model tests under three different noise models, Gaussian (black), bootstrapped residuals (red) and Laplacian (green). (C): QQ-plot of p-values derived from plain saturated model tests. Exactly valid null p-values would follow the theoretical* $U(0,1)$ *distribution (i.e., valid Type-I control) while optimistic (superuniform) p-values would lie below the diagonal (i.e., invalid Type-I control). (D): QQ-plot of p-values derived from our modified bootstrap substitution method that involves bootstrapping* $\boldsymbol{y} - \widehat{\boldsymbol{\theta}}$ *instead of* $\boldsymbol{y} - \bar{\boldsymbol{y}}$*. Note: this figure appears in color in the electronic version of this article, and any mention of color refers to that version Note: this figure appears in color in the electronic version of this article, and any mention of color refers to that version.*

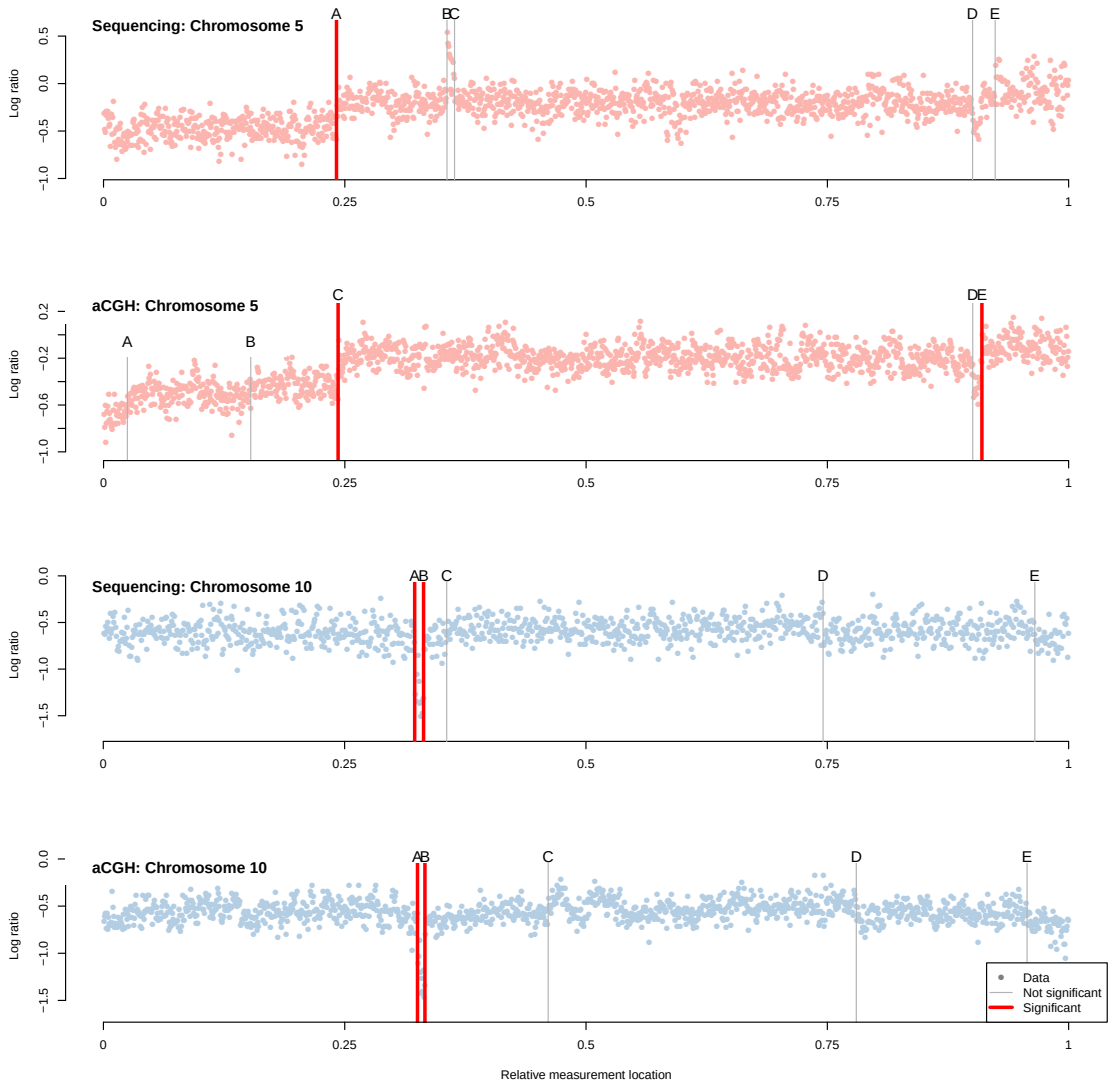

Figure 5: *Changepoint inference using saturated model tests for 5-step WBS marginalized over random intervals conducted over various chromosomes. In all the panels, the letters A through E denote the estimated changepoints, $\widehat{c}_1$ through $\widehat{c}_4$ respectively. The bolded gray (or red) horizontal lines denote changepoints that were rejected (or not rejected) under the null hypothesis The x-axis denotes the relative index of the genome position (normalized to be between 0 and 1) while the y-axis denotes the measured* $\log_2$ *copy number. (Top two panels): Analyses for chromosome 5 using sequencing data on the top and aCGH data on the bottom, where a significant changepoint around location 0.25 is shown (A and C respectively). However, in the aCGH analysis, changepoint E is deemed significant, which does not have a counterpart in the sequencing analysis. (Bottom two panels): Similar analysis but for chromosome 10, where changepoints A and B are marked significant between both data sources. These changepoints around location 0.3 is validated by FISH results Talevich et al. (2016). Note: this figure appears in color in the electronic version of this article, and any mention of color refers to that version.*

Biometrics 000, 000–000 DOI: 000
000 0000

Supporting Information: Post-Selection Inference for Changepoint Detection Algorithms with Application to Copy Number Variation Data

Sangwon Hyun*

Department of Data Sciences and Operations, University of Southern California, Los Angeles, CA.

email: shyun@usc.edu

and

Kevin Z. Lin

Department of Statistics, University of Pennsylvania, Philadelphia, PA.

and

Max G'Sell and Ryan J. Tibshirani

Department of Statistics and Data Science, Carnegie Mellon University, Pittsburgh, PA.

This paper has been submitted for consideration for publication in *Biometrics*

Supplementary Materials

A *Appendix summary*

The code to perform estimation as well as saturated model tests are in https://github.com/robohyun66/binseginf, while the code to perform selected model tests are additionally in https://github.com/linnyKos/selectiveModel. The datasets in this article were obtained from the following places: for the Snijder analysis (Section 4.1), we used the data directly from the GLAD Bioconductor package (https://www.bioconductor.org/packages/release/bioc/html/GLAD.html), and for the Botton analysis (Section 4.3), we used the aCGH data directly from the CNVkit example GitHub package (https://github.com/etal/cnvkit-examples) while we preprocessed the BAM files in the same package using the CNVkit software (https://github.com/etal/cnvkit) to obtain the sequencing data, using the steps outlined in the CNVkit example package.

The following is a brief summary of the supporting information.

Appendix B contains a concise summary of the all the practicalities and extensions of our inferential tools mentioned in the main text. Appendix C reviews circular binary segmentation (CBS) and fused lasso (FL) and provides analogous results of the polyhedron (which is novel for CBS, and is a review of existing results from Hyun et al. (2018) for FL). Appendix D contains the algorithmic details for the selected model test sampler in the known and unknown σ^2 setting, as well as details for the marginalized variants of the saturated model tests. Appendix E contains numerous simulations results and details, including more details of our simulation demonstrating that our inferential tools has more unconditional power than sample splitting in Section 3.4. Appendix F contains a description of the procedure to choose k adaptively and its corresponding simulation results. Appendix G contains additional results on our CNV applications. Appendix H contains the proofs to our theoretical results.

B *Practicalities and extensions*

The sections in the main text formalize the mechanisms to perform post-selective inference with respect to the basic procedure highlighted in Section 1. However, as we've alluded to in the main text, especially in the applications in Section 4, there are many choices and variants the researcher can choose from which can affect the results in practice. To ease researchers into using our inferential tools, we summarize all the combination of choices mentioned in this work that the user faces based on the methods developed in the above sections and their practical impact.

B.1 *Practical considerations.* There are some practical choices that the user needs to make when implementing the procedure. Here, we summarize these choice, as alluded to in Section 1.

- **Algorithm (BS, WBS, CBS and FL)**: FL and BS have similar mechansims, but BS has a simpler mechanism and a less complex selection event, potentially giving higher post-selection conditional power. CBS is specialized for pairs of changepoints, and WBS specializes in localized changepoint detection compared to BS, but both have higher computational burden due to their more complex polyhedra.
- **Conditioning** (Plain or marginalized): Marginalizing over a source of randomness yields tests with higher power than plain inference, but at two costs: increased computational burden due to MCMC sampling being required, and worsened detection ability when using additive noise marginalization. Also, the marginalized p-values are subject to the sampling randomness, and the number of trials T needed to reduce the p-values' intrinsic variability scales with σ^2_{add}.
- **Number of estimated changepoints k (Fixed or data-driven)**: As currently described in Section 2.1, we described methods to find a fixed number of changepoints k. However, we can adopt stopping rules from Hyun et al. (2018) to adaptively choose k.

This increases the complexity of the polyhedra compared to those in Section 3.1, leading to lower statistical power than its fixed-k counterpart. This is shown in Appendix F.

- **Assumed null model (Saturated or selected)**: As mentioned in Section 2.2, selected model tests are valid under a stricter set of assumptions but often yield higher power. Computationally, saturated model tests are often simpler to perform than selected model tests due to the closed form expression of the tail probability.
- **Error variance σ^2 (Known or unknown)**: Saturated model tests require σ^2 to be known. In practice, we need to estimate it in-sample from a reasonable changepoint mean fitted to the same data, or estimated out-of-sample on left-out data. Selected model tests have the advantage of not requiring knowledge of σ^2, but require a larger computational burden, as mentioned in Section 3.2.

B.2 *Extensions.* As mentioned in Hyun et al. (2018), there are many practically-motivated extensions to the baseline procedure mentioned in Section 1 to either improve power or interpretability. We highlight these below. All of these extensions will still give proper Type-I error control under the appropriate null hypotheses.

- **Designing linear contrasts**: The user can make many types of contrast vectors v to fit their analysis, in addition to the segment test contrasts (2), as long as it measurable with respect to $M(y_{\text{obs}})$. One example is the spike test from (Hyun et al., 2018) of single location mean changes. For CNV analysis, it could be useful to test regions between an adjacent pair of changepoints away from the immediately surrounding regions. Also, a step-sign plot (a plot that shows the locations and direction of the changepoints, but not their magnitude) can help the user design contrasts (Hyun et al., 2018).
- **Post-processing the estimated changepoints (Decluttering and screening)**: Multiple detected changepoints too close to one another can hurt the power of segment tests. Post-processing the estimated changepoints based on decluttering (Hyun et al., 2018) or

screening (Lin et al., 2017) so the new set of changepoints are well-separated can lead to contrasts that yield higher power. We show empirical evidence of this improving power of the fused lasso, in Appendix E.7.

- **Pre-cutting**: We can also modify all the algorithms in Section 2.1 to start with an initial existing set of changepoints. This is useful in CGH analyses, when it is not meaningful to consider segments that start in one chromosome and end in another. By pooling information in this manner from separate chromosomal regions, the pre-cut analysis is an improvement over conducting separate analyses in individual chromosomes.

C *Circular binary segmentation and fused lasso*

Below, we review circular binary segmentation (CBS) and fused lasso (FL), as well as the analogous results for their respective polyhedra $\mathbf{\Gamma}$. To clarify, our results for CBS are novel, but our results for FL are taken directly from Hyun et al. (2018). We also include more discussion between all four methods – BS, WBS, CBS and FL.

We additionally note that all the algorithms we mention in our article is sometimes written differently in other changepoint work. Specifically, these algorithms (BS, WBS, and CBS) are sometimes described in the literature as recursively running until internally calculated statistics do not exceed a given threshold level τ. The reason that we choose to instead describe them as running until k steps is two-fold. First, we feel it is easier for a user to specify a priori a reasonable number of steps k, versus a threshold level τ. Second, we can use the method in Hyun et al. (2018) to adaptively choose the number of steps k and still perform valid inferences.

C.1 *Methods.*

The following descriptions are a continuation of the discussions in Section 2.1.

Circular binary segmentation (CBS). The k-step CBS algorithm (Olshen et al., 2004) specializes in detecting *pairs* of changepoints that have alternating directions. At a

step $\ell = 1, \ldots, k$, let $\widehat{\boldsymbol{a}}_{1:(\ell-1)}$, $\widehat{\boldsymbol{b}}_{1:(\ell-1)}$ be the changepoints estimated so far (with the pair a_j, b_j estimated at step j), and let $\boldsymbol{I}_j$, $j = 1, \ldots, 2\ell+1$ be the associated partition of $\{1, \ldots, n\}$. Intervals of length 2 are discarded. Let s_j and e_j denote the start and end index of $\boldsymbol{I}_j$. The next changepoint pair $\widehat{a}_\ell$ and $\widehat{b}_\ell$, and the maximizing interval index $\widehat{j}_\ell$, are found by

$$\{\widehat{j}_\ell, \widehat{a}_\ell, \widehat{b}_\ell\} = \underset{\substack{j \in \{1,\ldots,2(\ell-1)+1)\} \\ a,b \in \{s_j,\ldots,e_j-1\} \,:\, a<b}}{\operatorname{argmax}} \left|\boldsymbol{g}_{(s_j,a,b,e_j)}^T \boldsymbol{y}\right| \quad \text{where} \tag{1}$$

$$\boldsymbol{g}_{(s,a,b,e)}^T \boldsymbol{y} = \sqrt{\frac{1}{\frac{1}{|b-a|} + \frac{1}{|e-s-b+a|}}} \Big(\overline{y}_{(a+1):b} - \overline{y}_{\{s:a\} \cup \{(b+1):e\}} \Big). \tag{2}$$

As before, the new changepoint direction $\widehat{d}_\ell$ is defined based on the sign of the (modified) CUSUM statistic, $\widehat{d}_\ell = \operatorname{sign}(\boldsymbol{g}_{(s_j,a_{\ell+1},b_{\ell+1},e_j)}^T \boldsymbol{y})$ for $j = \widehat{j}_{\ell+1}(\boldsymbol{y})$.

Fused lasso (FL). The fused lasso estimator is defined by solving the convex optimization problem,

$$\min_{\theta \in \mathbb{R}^n} \sum_{i=1}^n (y_i - \theta_i)^2 + \lambda \sum_{i=1}^{n-1} |\theta_i - \theta_{i+1}|, \tag{3}$$

for a tuning parameter $\lambda \geqslant 0$. The fused lasso can be seen as a k-step algorithm by sweeping the tuning parameter from $\lambda = \infty$ down to $\lambda = 0$. Then, at given values of λ (called knots), the FL estimator sequentially introduces an additional changepoint into the solution of (3). See Hyun et al. (2018) for a more in-depth description.

C.2 *Polyhedral selection events for CBS and FL.* The following descriptions are a continuation of the discussions in Section 3.1. We prove the polyhedral selection event for CBS below, as well as review the existing result about the polyhedral selection event for FL.

Selection event for CBS. We define the model for the k-step CBS estimator as

$$M_{1:k}^{\mathrm{CBS}}(\boldsymbol{y}_{\mathrm{obs}}) = \big\{\widehat{\boldsymbol{a}}_{1:k}(\boldsymbol{y}_{\mathrm{obs}}),\ \widehat{\boldsymbol{b}}_{1:k}(\boldsymbol{y}_{\mathrm{obs}}),\ \widehat{\boldsymbol{d}}_{1:k}(\boldsymbol{y}_{\mathrm{obs}})\big\},$$

where now $\widehat{\boldsymbol{a}}_{1:k}(\boldsymbol{y}_{\mathrm{obs}})$ and $\widehat{\boldsymbol{b}}_{1:k}(\boldsymbol{y}_{\mathrm{obs}})$ are the pairs of estimated changepoint locations, and $\widehat{\boldsymbol{d}}_{1:k}(\boldsymbol{y}_{\mathrm{obs}})$ are the changepoint directions, as described in Section 2.1.

PROPOSITION 1: *Given any fixed $k \geqslant 1$ and $\{\boldsymbol{a}_{1:k}, \boldsymbol{b}_{1:k}, \boldsymbol{d}_{1:k}\}$, we can explicitly construct*

$\boldsymbol{\Gamma}$ *where*

$$\big\{\boldsymbol{y} : M^{\mathrm{CBS}}_{1:k}(\boldsymbol{y}, \boldsymbol{w}) = \{\boldsymbol{a}_{1:k}, \boldsymbol{b}_{1:k}, \boldsymbol{d}_{1:k}\}\big\} = \big\{\boldsymbol{y} : \boldsymbol{\Gamma}\boldsymbol{y} \geqslant \boldsymbol{0}\big\}.$$

Let $\boldsymbol{I}^{(\ell)}_j$ *denote the* j*th interval of* $B(\ell)$ *intervals remaining for an intermediate step* $\ell \in \{1, \ldots, k\}$*, and let* $C(x, 2) = \binom{x}{2}$*. Then* $\boldsymbol{\Gamma}$ *has a number of rows equal to*

$$2\sum_{\ell=1}^{k}\Big\{\sum_{j=1}^{B(\ell)} C(|\boldsymbol{I}^{(\ell)}_j| - 1, 2) - 1\Big\}.$$

Selection events for FL, and a brief comparison. The model for the k-step FL estimator is

$$M^{\mathrm{FL}}_{1:k}(\boldsymbol{y}_{\mathrm{obs}}) = \big\{\widehat{\boldsymbol{b}}_{1:k}(\boldsymbol{y}_{\mathrm{obs}}),\ \widehat{\boldsymbol{d}}_{1:k}(\boldsymbol{y}_{\mathrm{obs}}),\ \widehat{\boldsymbol{R}}_{1:k}(\boldsymbol{y}_{\mathrm{obs}})\big\},$$

where $\widehat{\boldsymbol{b}}_{1:k}(\boldsymbol{y})$ and $\widehat{\boldsymbol{d}}_{1:k}(\boldsymbol{y})$ are changepoint locations and directions, and $\widehat{\boldsymbol{R}}_{\ell}(\boldsymbol{y}) \in \mathbb{R}^{n-\ell}$ for $\ell = 1, \ldots, k$ whose elements represent signs of a certain statistic $h_i(\boldsymbol{y})$ calculated at location i in competition for maximization with $\widehat{\boldsymbol{b}}_{\ell}$ at step ℓ. These statistics $h_i(\boldsymbol{y})$ are weighted mean differences at location i and are analogous to CUSUM statistics in BS. Hyun et al. (2018) makes this representation more explicit, proving that for any fixed $k \geqslant 1$ and $\boldsymbol{b}_{1:k}, \boldsymbol{d}_{1:k}, \boldsymbol{R}_{1:k}$, we can explicitly construct $\boldsymbol{\Gamma}$ such that

$$\big\{\boldsymbol{y} : M^{\mathrm{FL}}_{1:k}(\boldsymbol{y}) = \{\boldsymbol{b}_{1:k}, \boldsymbol{d}_{1:k}, \boldsymbol{R}_{1:k}\}\big\} = \{\boldsymbol{y} : \boldsymbol{\Gamma}\boldsymbol{y} \geqslant \boldsymbol{0}\},$$

where $\boldsymbol{\Gamma}$ has the same number of rows as a k-step BS event.

D *Additional algorithmic details*

In this section, we describe additional algorithmic details for selected model tests (from Section 3.2) and marginalized saturated tests (from Section 3.3).

D.1 *Selected model tests, hit-and-run sampling for known* σ^2*.* The following is the hit-and-run sampler to estimate the tail probability of the law of (5). This is for the known σ^2 setting, which differs from the setting described in the main text in Section 3.2. This was briefly described in Fithian et al. (2015) but the authors have later implemented it in ways not

originally described in the above works to make it more efficient. We do not claim novelty for the following algorithm, but simply state it for completion. The original code can be found the repository https://github.com/selective-inference, and we reimplemented it to suite our coding framework and simulation setup.

We specialize our description to test the null hypothesis $H_0 : \boldsymbol{v}_j^T \boldsymbol{\theta} = 0$ against the one-sided alternative $H_1 : \boldsymbol{v}_j^T \boldsymbol{\theta} > 0$. There are some notation to clarify prior to describing the algorithm. Let $\boldsymbol{v}_j \in \mathbb{R}^n$ denote the vector such that

$$\boldsymbol{v}_j^T \boldsymbol{y} = \overline{y}_{\boldsymbol{I}_{j+1}} - \overline{y}_{\boldsymbol{I}_j}.$$

Let $\boldsymbol{A} \in \mathbb{R}^{k \times n}$ denote the matrix such that the last k equations in the above display are satisfied if and only if $\boldsymbol{AY} = \boldsymbol{A}\boldsymbol{y}_{\text{obs}}$. Based on Section 3.1, observe that our goal reduces to sampling from the n-dimensional distribution

$$\boldsymbol{Y} \sim \mathcal{N}(\boldsymbol{0}, \sigma^2 \boldsymbol{I}_n), \quad \text{conditioned on} \quad \boldsymbol{\Gamma Y} \geqslant \boldsymbol{0},\ \boldsymbol{AY} = \boldsymbol{A}\boldsymbol{y}_{\text{obs}}. \tag{4}$$

where $\boldsymbol{I}_n$ is the $n \times n$ identity matrix. (Observe that we can set the mean of the above Gaussian distribution to any vector $\boldsymbol{\theta}$ as long as $\boldsymbol{\theta}$ satisfies the null hypothesis. We choose $\boldsymbol{\theta} = \boldsymbol{0}$ for convenience here.)

The first stage of the algorithm *removes the nullspace* of $\boldsymbol{A}$ in the following sense. Construct any matrix $\boldsymbol{B} \in \mathbb{R}^{n \times n}$ such that it has full rank and the last k rows are equal to $\boldsymbol{A}$. Then, consider the following n-dimensional distribution.

$$\boldsymbol{Y}' \sim \mathcal{N}(\boldsymbol{0}, \sigma^2 \boldsymbol{B}^T \boldsymbol{B}), \quad \text{conditioned on} \quad \boldsymbol{\Gamma B}^{-1} \boldsymbol{Y}' \geqslant \boldsymbol{0},\ (\boldsymbol{Y}')_{(n-k+1):n} = \boldsymbol{A}\boldsymbol{y}_{\text{obs}}. \tag{5}$$

Note that $\boldsymbol{B}^{-1}\boldsymbol{Y}'$ has the same law as (8). Observe that the above distribution is a conditional Gaussian, meaning we can remove the last conditioning event. Towards that end, let $\boldsymbol{\Gamma}''$ denote the first $n-k$ columns of the matrix $\boldsymbol{\Gamma B}^{-1}$, and let $\boldsymbol{u}''$ denote the last k columns of $\boldsymbol{\Gamma B}^{-1}$ left-multiplying $\boldsymbol{A}\boldsymbol{y}_{\text{obs}}$. Also, consider the following partitioning of the matrix $\boldsymbol{B}^T\boldsymbol{B}$,

$$\sigma^2 \cdot \boldsymbol{B}^T \boldsymbol{B} = \begin{bmatrix} \boldsymbol{B}_{11} & \boldsymbol{B}_{12} \\ \boldsymbol{B}_{12}^T & \boldsymbol{B}_{22} \end{bmatrix},$$

where $\boldsymbol{B}_{11}$ is a $(n-k)\times(n-k)$ submatrix, $\boldsymbol{B}_{12}$ is a $(n-k)\times k$ submatrix, and $\boldsymbol{B}_{22}$ is a $k\times k$ submatrix. Then, consider the following $n-k$-dimensional distribution.

$$\boldsymbol{Y}'' \sim \mathcal{N}\Big(\boldsymbol{B}_{12}\boldsymbol{B}_{22}^{-1}(\boldsymbol{A}\boldsymbol{y}_{\text{obs}}),\ \boldsymbol{B}_{11}-\boldsymbol{B}_{12}\boldsymbol{B}_{22}^{-1}\boldsymbol{B}_{12}^{T}\Big), \quad \text{conditioned on} \quad \boldsymbol{\Gamma}''\boldsymbol{Y}'' \geqslant -\boldsymbol{u}''. \tag{6}$$

Note that $\boldsymbol{Y}''$ has the same law as the first $n-k$ coordinates of (5).

The next stage of the algorithm *whitens* the above distribution so its covariance is the identity. Let $\boldsymbol{\mu}''$ and $\boldsymbol{\Sigma}''$ denote the mean and variance of the unconditional form of the above distribution (6). Let $\boldsymbol{\Theta}$ be the matrix such that $\boldsymbol{\Theta}\boldsymbol{\Sigma}''\boldsymbol{\Theta}^{T}=\boldsymbol{I}_n$. This must exist since $\boldsymbol{\Sigma}''$ is positive definite. Consider the following $n-k$ dimensional distribution,

$$\boldsymbol{Z} \sim \mathcal{N}(\boldsymbol{0},\boldsymbol{I}_n), \quad \text{conditioned on} \quad \boldsymbol{\Gamma}''\boldsymbol{\Theta}^{-1}\boldsymbol{Z} \geqslant -\boldsymbol{u}''-\boldsymbol{\Gamma}''\boldsymbol{\mu}''. \tag{7}$$

Note that $\boldsymbol{\Theta}^{-1}\boldsymbol{Z}+\boldsymbol{\mu}''$ has the same law as (6). Hence, we have constructed linear mappings F and G between (8) and (7) such that $F(\boldsymbol{Y}) \overset{d}{=} \boldsymbol{Z}$, and $G(\boldsymbol{Z}) \overset{d}{=} \boldsymbol{Y}$ (i.e., have the same distribution).

In order to set up a hit-and-run sampler, generate p unit vectors $\boldsymbol{g}_1,\ldots,\boldsymbol{g}_p$. (The choice of p is arbitrary, and the specific method of generating these p vectors is also arbitrary.) Our hit-and-run sampler will move in the linear directions dictated by $\boldsymbol{g}_1,\ldots,\boldsymbol{g}_p$. We are now ready to describe the hit-and-run sampler in Algorithm 1, which leverages many of the same calculations in (8) and (9) (from Section 3.2). The similarity arises since conditional slices of a multivariate Gaussian still yield Gaussian distributions (loosely speaking), and $\Pi^{\perp}_{\boldsymbol{g}_i}(\boldsymbol{Z}+\boldsymbol{g}_i)=\Pi^{\perp}_{\boldsymbol{g}_i}\boldsymbol{Z}$ (by definition of projections).

The computational efficiency of Algorithm 1 comes from the fact that very few multiplication operations need to be done with the polyhedron matrix $\boldsymbol{\Gamma}''\boldsymbol{\Theta}^{-1}$, a potentially huge matrix. $\boldsymbol{U}$ and $\boldsymbol{\rho}_1,\ldots,\boldsymbol{\rho}_p$ (each vectors of the same length to be defined in the algorithm below) carry all the information needed about polyhedron throughout the entire procedure of generating M samples.

Algorithm 1: MCMC hit-and-run algorithm for selected model test with known σ^2

Choose a number M of iterations.

Set $\boldsymbol{z}^{(0)} = F(\boldsymbol{y}_{\text{obs}})$, as described in the text.

Generate p unit directions $\boldsymbol{g}_1, \ldots, \boldsymbol{g}_p$, each vector of length n.

Compute $\boldsymbol{U} = \boldsymbol{\Gamma}''\boldsymbol{\Theta}^{-1}\boldsymbol{z}^{(0)} + \boldsymbol{u}'' + \boldsymbol{\Gamma}''\boldsymbol{\mu}''$, which represents the "slack" of each constraint.

Compute the p vectors, $\boldsymbol{\rho}_i = \boldsymbol{\Gamma}''\boldsymbol{\Theta}^{-1}\boldsymbol{g}_i$ for $i \in \{1, \ldots, p\}$.

for $m \in \{1, \ldots, M\}$ **do**

Select an index i uniformly from 1 to p.

Compute the truncation bounds

$$\mathcal{V}_{\text{lo}} = \boldsymbol{g}_i^T\boldsymbol{z}^{(m-1)} - \min_{j:(\boldsymbol{\rho}_i)_j > \boldsymbol{0}} U_j/(\boldsymbol{\rho}_i)_j, \quad \text{and} \quad \mathcal{V}_{\text{up}} = \boldsymbol{g}_i^T\boldsymbol{z}^{(m-1)} - \max_{j:(\boldsymbol{\rho}_i)_j < \boldsymbol{0}} U_j/(\boldsymbol{\rho}_i)_j.$$

Sample $\boldsymbol{\alpha}^{(m)}$ from a Gaussian with mean $\boldsymbol{g}_i^T\boldsymbol{z}^{(m-1)}$ and variance 1, truncated to lie between $\mathcal{V}_{\text{lo}}$ and $\mathcal{V}_{\text{up}}$.

Form the next sample

$$\boldsymbol{z}^{(m)} = \boldsymbol{z}^{(m-1)} + \boldsymbol{\alpha}^{(m)}\boldsymbol{g}_i, \quad \text{and} \quad \boldsymbol{y}^{(m)} = G(\boldsymbol{z}^{(m)}).$$

Update the slack variable,

$$\boldsymbol{U} \leftarrow \boldsymbol{U} + \boldsymbol{\alpha}^{(m)}\boldsymbol{\rho}_i.$$

Return the approximate for the tail probability of (6), $\sum_{m=1}^{M} \mathbb{1}[\boldsymbol{v}^T\boldsymbol{y}^{(m)} \geqslant \boldsymbol{v}^T\boldsymbol{y}_{\text{obs}}]/M$.

D.2 *Selected model tests, hit-and-run sampling for unknown σ^2.* Below in Algorithm 2, we explicitly describe the hit-and-run sampler we developed to perform selected model tests for unknown σ^2, described in Section 3.2. Similar to the previous subsection, for notational convenience, observe that the last k constraints in (10) can be rewritten as $\boldsymbol{AY} = \boldsymbol{A}\boldsymbol{y}_{(\text{obs})}$ for some matrix $\boldsymbol{A} \in \mathbb{R}^{k\times n}$. Recall that our goal in this setting is to sample from the distribution

$$\boldsymbol{Y} \sim \mathcal{N}(\boldsymbol{0}, \boldsymbol{I}_n), \quad \text{conditioned on} \quad \boldsymbol{\Gamma Y} \geqslant \boldsymbol{0},\ \boldsymbol{AY} = \boldsymbol{A}\boldsymbol{y}_{\text{obs}},\ \|\boldsymbol{Y}\|_2 = \|\boldsymbol{y}_{\text{obs}}\|_2. \tag{8}$$

Similar to the above subsection, observe that the mean vector $\boldsymbol{\theta}$ of the Gaussian distribution is arbitrary as long as the null hypothesis is satisfied (and hence we denote $\boldsymbol{\theta} = \mathbf{0}$ for convenience) and the covariance matrix $\boldsymbol{\Sigma}$ of the Gaussian distribution is also arbitrary as long as it is a diagonal matrix since we are conditioning on the event $\|\boldsymbol{Y}\|_2 = \|\boldsymbol{y}_{\text{obs}}\|_2$ (and hence we denote $\boldsymbol{\Sigma} = \boldsymbol{I}_n$ for convenience). As described in the paper, since we are conditioning on all the sufficient statistics under the null hypothesis, sampling from the above distribution is equivalent to sampling uniformly from the set

$$\Big\{\boldsymbol{Y} : \boldsymbol{\Gamma Y} \geqslant \mathbf{0},\ \boldsymbol{AY} = \boldsymbol{A}\boldsymbol{y}_{\text{obs}},\ \|\boldsymbol{Y}\|_2 = \|\boldsymbol{y}_{\text{obs}}\|_2\Big\},$$

which is the goal of the hit-and-run sampler below.

Algorithm 2: MCMC hit-and-run algorithm for selected model test with unknown σ^2

Choose a number M of iterations and set $\boldsymbol{y}^{(0)} = \boldsymbol{y}_{\text{obs}}$.

for $m \in \{1, \ldots, M\}$ **do**

Uniformly sample two unit vectors $\boldsymbol{s}$ and $\boldsymbol{t}$ in the nullspace of $\boldsymbol{A}$.

Compute the set $\mathcal{I} \subseteq [-\pi/2, \pi/2]$ that intersects the set

$$\Big\{\boldsymbol{y} \ :\ \boldsymbol{y} = \boldsymbol{y}^{(m-1)} + r(\omega)\sin(\omega)\cdot\boldsymbol{s} + r(\omega)\cos(\omega)\cdot\boldsymbol{t} \quad \text{for any } \omega \in [-\pi/2, \pi/2]\Big\},$$

for the radius function $r(\omega) = -2(\boldsymbol{y}^{(m-1)})^T(\sin(\omega)\cdot\boldsymbol{s} + \cos(\omega)\cdot\boldsymbol{t})$, with the polyhedral set implied by model selection event,

$$\Big\{\boldsymbol{y} \ :\ \boldsymbol{\Gamma y} \geqslant \mathbf{0}\Big\}.$$

Uniformly sample $\omega^{(m)}$ from $\mathcal{I}$ and form the next sample

$$\boldsymbol{y}^{(m)} = \boldsymbol{y}^{(m-1)} + r(\omega^{(m)})\sin(\omega^{(m)})\cdot\boldsymbol{s} + r(\omega)\cos(\omega^{(m)})\cdot\boldsymbol{t}.$$

Return the approximate for the tail probability of (7), $\sum_{m=1}^{M}\mathbb{1}[\boldsymbol{v}^T\boldsymbol{y}^{(m)} \geqslant \boldsymbol{v}^T\boldsymbol{y}_{\text{obs}}]/M$.

Observe that the set $\mathcal{I}$ in each iteration of the above algorithm can be a disjoint set of closed intervals in $[-\pi/2, \pi/2]$.

D.3 *Marginalization over additive noise or over WBS intervals.* In this section, we explicitly describe the algorithms to perform marginalized saturated model tests developed in Section 3.3. The two methods, marginalization over additive noise or over WBS intervals, are strikingly similar. In this section, we use the notation in Section 3.3, where

$$k(\boldsymbol{w}_{\text{obs}}) = \Phi\big(\mathcal{V}_{\text{up}}/\tau\big) - \Phi\big(\boldsymbol{v}^T\boldsymbol{y}_{\text{obs}}/\tau\big)$$
$$g(\boldsymbol{w}_{\text{obs}}) = \Phi\big(\mathcal{V}_{\text{up}}/\tau\big) - \Phi\big(\mathcal{V}_{\text{lo}}/\tau\big),$$

and in this marginalized setting,

$$\mathcal{V}_{\text{lo}} = \boldsymbol{v}^T\big(\boldsymbol{y}_{\text{obs}} + \boldsymbol{w}_{\text{obs}}\big) - \min_{j:\rho_j>0}\big\{\boldsymbol{\Gamma}(\boldsymbol{y}_{\text{obs}} + \boldsymbol{w}_{\text{obs}}\big\}_j/\rho_j,$$
$$\mathcal{V}_{\text{up}} = \boldsymbol{v}^T\big(\boldsymbol{y}_{\text{obs}} + \boldsymbol{w}_{\text{obs}}\big) - \max_{j:\rho_j<0}\big\{\boldsymbol{\Gamma}(\boldsymbol{y}_{\text{obs}} + \boldsymbol{w}_{\text{obs}})\big\}_j/\rho_j,$$

and $\tau = \sigma^2\|\boldsymbol{v}\|_2^2$ and $\boldsymbol{\rho} = \boldsymbol{\Gamma}\boldsymbol{v}/\|\boldsymbol{v}\|_2^2$.

First, in Algorithm 3, we describe the saturated model tests, marginalized over additive noise.

Algorithm 3: Marginalizing over additive noise

Choose a number T of trials.

for $t \in \{1, \dots, T\}$ **do**

Sample the additive noise $\boldsymbol{w}_j$ from $\mathcal{N}(\boldsymbol{0}, \sigma^2_{\text{add}}\boldsymbol{I}_n)$.

Compute $k(\boldsymbol{w}_t)$ and $g(\boldsymbol{w}_t)$.

Return the approximate for the tail probability (12), $\sum_{t=1}^T k(\boldsymbol{w}_t)/\sum_{t=1}^T g(\boldsymbol{w}_t)$.

Next, in Algorithm 4, describe the saturated model tests, marginalized over WBS intervals.

Algorithm 4: Marginalizing over random intervals

Choose a number T of trials.

for $t \in \{1, \ldots, T\}$ **do**

Sample the non-maximizing intervals $\boldsymbol{w}_\ell = (s_\ell, \ldots, e_\ell)$ for $\ell \in \{1, \ldots, B\} \backslash \{\widehat{j}_{1:k}\}$ where s_ℓ, e_ℓ are uniformly drawn from 1 to n and $s_\ell < e_\ell$.

Check to see that $\{\widehat{j}_{1:k}\}$ are still the indices of the maximizing intervals. If not, return to the previous step.

Compute $k(\boldsymbol{w}_t)$ and $g(\boldsymbol{w}_t)$.

Return the approximate for the tail probability (12), $\sum_{t=1}^{T} k(\boldsymbol{w}_t) / \sum_{t=1}^{T} g(\boldsymbol{w}_t)$.

E *Simulations*

In this section, we show simulation examples to demonstrate properties of the segmentation post-selection inference tools presented in the current article.

E.1 *Data generating process.* Let the mean $\boldsymbol{\theta}$ consist of two alternating-direction change-points of size δ in the middle as in (9), chosen to be a realistic example of mutation phenomena as observed in aCGH datasets (Snijders et al., 2001). Specifically, let the sample size be set to be $n = 200$, chosen to be in the scale of the chromosomal data. Then, we model this using the equation below,

$$\textbf{Middle mutation: } \text{for } i \in 1, \ldots, n: \quad y_i \sim \mathcal{N}(\theta_i, 1), \quad \theta_i = \begin{cases} \delta & \text{if } 101 \leqslant i \leqslant 140 \\ 0 & \text{if otherwise,} \end{cases} \tag{9}$$

for the signal size $\delta \in \{0, 0.25, 0.5, 1, 2, 4\}$ with noise level $\sigma^2 = 1$.

E.2 *Methodology.* In the following simulations, we consider the following four estimators (BS, WBS, CBS and FL), each run for two steps. We perform saturated model tests on each estimator, but only perform selected model tests on BS and FL for simplicity, for both known and unknown noise parameter σ^2. We use the basis procedure outlined in Section 1 with a significance level of $\alpha = 0.05$. Throughout the entire simulation suite, the empirical

standard deviation in each of the power curves and detection probabilities is less than 0.02. For each method, for each signal-to-noise size δ, we run more than 250 trials.

E.3 *Type-I error control verification.* First, we examine all our statistical inferences under the global null where $\boldsymbol{\theta} = \mathbf{0}$ to demonstrate their validity – uniformity of null p-values, or type I error control. Specifically, any simulations from the no-signal regime $\delta = 0$ from the middle mutation (9) can be used. When there is no signal, the null scenario $\boldsymbol{v}^T\boldsymbol{\theta} = 0$ is always true so we expect all p-value to be uniformly distributed between 0 and 1. We verify this expected behavior in Figure 1. We notice that the methods that require MCMC (marginalized saturated and selected model tests) requires more trials to converge towards the uniform distribution compared to their counterparts that have exact calculations.

[Figure 1 about here.]

E.4 *Calculating power.* After verifying that our inferential tools have valid Type-I control, we now want to investigate their power – how often they correctly deem an estimated changepoint as significant when it is near a true changepoint. Since the tests are performed only when a changepoint is selected, it is necessary to separate the detection ability of the estimator from power of the test. To this end, we define the following quantities,

$$\text{Conditional power} = \frac{\#\text{ correctly detected \& rejected}}{\#\text{ correctly detected}} \tag{10}$$

$$\text{Detection probability} = \frac{\#\text{ correctly detected}}{\#\text{ tests conducted}} \tag{11}$$

$$\text{Unconditional power} = \text{Detection} \times \text{Conditional power} \tag{12}$$

The overall power of an inference tool can only be assessed by examining the conditional and unconditional power together. We consider a detection to be correct if it is within ± 2 of the true changepoint locations.

E.5 *Power comparison across signal sizes δ.* For saturated model tests, we perform additive-noise inferences using Gaussian $\mathcal{N}(0, \sigma^2_{\text{add}})$ with $\sigma_{\text{add}} = 0.2$ for BS, FL, and CBS. For WBS, we employ the randomization scheme as described in Section 3.3 with $B = n$. With the metrics in (11)-(12), we examine the performance of the four methods. The solid lines in Figure 2 show the "plain" method where model selection based on $M(y_{\text{obs}})$. The dotted lines show the marginalized counterparts where the model selection is $M(y_{\text{obs}}, W)$, margnialized over W.

We see in Figure 2 that WBS and CBS have higher conditional and unconditional power than BS. This is expected since the former two are more adept for localized change-points of alternating directions. FL noticeably under-performs in power compared to segmentation methods. This is partially caused by FL's detection behavior, and can be explained by examining alternative measures of detection and improved with post-processing. This investigation is deferred to Appendix E.7. The marginalized versions of each algorithm have noticeably improved power, but almost unnoticeably worse detection than their non-randomized, plain versions (middle panel of Figure 2). Combined, in terms of unconditional power, marginalized inferences clearly dominate their plain counterparts.

Selected model inference simulations are shown in Figure 3. Surprisingly, there is an almost inconceivable drop in power from unknown σ^2 to known σ^2. Compared to the saturated model tests in Figure 2, there is smaller power gap between FL and BS. Also, selected model tests appear to have higher power than saturated model tests. In general however, it is hard to compare the power of saturated and selected models due to the clear difference in model assumptions.

[Figure 2 about here.]

[Figure 3 about here.]

E.6 *More details about sample splitting.* Here, we discuss the details used to generate Figure 2. As mentioned in the main text, sample splitting is another valid inference technique. After splitting the dataset in half based on even and odd indices, we run a changepoint algorithm on one dataset and conduct classical one-sided t-test on the other. This is the most comparable test, as it does not assume σ^2 is known and conducts a one-sided test of the null $H_0 : \boldsymbol{v}^T\boldsymbol{\theta} = 0$. Instead of ± 2 slack used for calculating detection in post-selective inference (dotted and dashed lines), ± 1 was used for sample splitting inference (solid line). The loss in detection accuracy in the middle panel of Figure 2 shows the downside of halving data size for detection. Unconditional power for marginalized saturated model tests and selected model tests are noticeably higher than the other two.

We note that the results in Figure 2 were based on approximate detection. This choice of approximate detection is somewhat arbitrary, and it is informative to see if the results would change if we considered only exact detection. We can see from Figure 4 that randomized TG p-values have comparable power with sample splitting inferences, among tests that are regarding exactly the right changepoints.

[Figure 4 about here.]

E.7 *Power comparison using unique detection.* FL was appeared to have a large drop in power compared to segmentation algorithms. In addition to these three measures shown in Appendix E.4, for multiple changepoint problems like middle mutations it is useful to measure performance using an alternative measure of detection called unique detection. This is useful because some algorithms – mainly FL, but to also BS to some extent, primarily in later steps – admit "clumps" of nearby points. If this clumped detection pattern occurs in early steps, the algorithm requires more steps than others to fully admit the correct changepoints. In this case, detection alone is not an adequate metric, and unique detection

can be used in place.

$$\text{Unique detection probability} = \frac{\#\text{changepoints which were approximately detected}}{\#\text{number of true changepoints.}} \quad (13)$$

In plain words, unique detection is measuring how many of the true changepoint locations have been approximately recovered.

We present a simple case study. In addition to a 2-step FL, imagine using a 3-step FL, but with post-processing. For post-processing, declutter by centroid clustering with maximum distance of 2, and test the $k_0 < 3$ changepoints, pitting the resulting segment test p-values against $0.05/k_0$. A 2-step FL's detection does not reach 1 even at high signals ($\delta = 4$) because of the aforementioned clumped detection behavior. The resulting segment tests are also not powerful, since the segment test contrast vectors consist of left and right segments which do not closely resemble true underlying piecewise constant segments in the data. However, when detection is replaced with unique detection, two things are noticeable. First, decluttered FL's detection performance is noticeably improved when going from 2 to 3 steps. Also, when unconditional power is calculated using unique detection, BS does not have as large of an advantage over the the several variants of fused lasso. This is shown in Figure 5. We see from the right figure (compared to the left) that the a "decluttered" version of 2- or 3-step FL has much closer unconditional power to BS.

[Figure 5 about here.]

E.8 *Power comparison with different mean shape.* The synthetic mean discussed here consists of a single upward changepoint piece-wise constant mean, as shown in (14) and Figure 6 (right). This is chosen to be another realistic example of the mutation phenomenon as observed in aCGH datasets from Snijders et al. (2001), in addition to the case shown in the main text. We focus on the *duplication* mutation scenario, but the results apply similarly to deletions. As before, the sample size $n = 200$ was chosen to be in the scale of the data length in a typical aCGH dataset in a single chromosome. For saturated model tests, WBS

no longer outperforms BS in power. This is expected since there is only a single changepoint not accompanied by opposing-direction changepoints.

$$\textbf{Edge mutation:} \quad y_i \sim \mathcal{N}(\theta_i, 1), \;\; \theta_i = \begin{cases} \delta & \text{if } 161 \leqslant i \leqslant 200 \\ 0 & \text{if otherwise} \end{cases} \tag{14}$$

[Figure 6 about here.]

[Figure 7 about here.]

F *Model size selection using information criteria – choosing k adaptively*

Throughout the article we assume that the number of algorithm steps k is fixed. Hyun et al. (2018) introduces a stopping rule based on information criteria (IC) which can be characterized as a polyhedral selection event. The IC for the sequence of models $M_{1:\ell}$, for $\ell = 1, \ldots, n-1$ is

$$J(M_{1:\ell}) = \|\boldsymbol{y} - \widehat{\boldsymbol{y}}_{M_{1:\ell}(\boldsymbol{y})}\|_2^2 + p\big(M_{1:\ell}(\boldsymbol{y})\big). \tag{15}$$

We omit the dependency on $\boldsymbol{y}$ when obvious. We use the BIC complexity penalty $p(M_k) = \sigma^2 \cdot k \cdot \log(n)$ for this article. Also define $S_\ell(\boldsymbol{y}) = \text{sign}\left(J(M_{1:\ell}) - J(M_{1:(\ell-1)})\right)$ to be the sign of the difference in IC between step $\ell - 1$ and ℓ. This is a $+1$ for a rise and -1 for a decline. A data-dependent stopping rule $\widehat{k}$ is defined as

$$\widehat{k}(y) = \min\{k : S_k(y) = S_{k+1}(y) = \ldots = S_{k+q}(y) = 1\} \tag{16}$$

which is a local minimization of IC, defined as the first time q consecutive rises occur. As discussed in Hyun et al. (2018), $q = 2$ is a reasonable choice for the changepoint detection. To carry out valid post-selective inference, we condition on the selection event $\mathbb{1}[S_{1:(k+q)}(\boldsymbol{y}) = S_{1:(k+q)}(\boldsymbol{y}_{\text{obs}})]$, which is enough to determine $\widehat{k}$. A k-step model for k chosen by (16) can be understood to be $M_{1:\widehat{k}}(\boldsymbol{Y}) = M_{1:k}(\boldsymbol{y}_{\text{obs}})$. The corresponding selection event $P_{M_{1:\widehat{k}}}$ is with the additional halfspaces, as outlined in Hyun et al. (2018). Simulations in Figure 8 show

that introducing IC stopping is valid, by controlled type-I error, but comes at the cost of considerable power loss.

[Figure 8 about here.]

G *Additional results to CNV analyses in Section 4*

G.1 *Additional details to Snijders analysis in Section 4.1.* In this section, we provide additional details associated with results in Section 4.1. As part of the preprocessing, we also remove single outliers which are at least three standard deviations away from its surrounding points. Afterwards, we set σ^2 for all the saturated model tests in that section for a particular cell line by computing the empirical variance after fitting a pre-cut 10-step WBS across said cell line.

G.2 *Additional details and results to follow-up analysis of Snijders dataset in Section 4.2.* In this section, we provide additional details and results associated with the heavy-tail study performed in Section 4.2. Throughout all the simulations in that section, we set σ^2 for all the saturated model tests by computing the empirical variance after fitting a pre-cut 10-step WBS across the entire cell line GM01750.

We had mentioned the bootstrap substitution method proposed by Tibshirani et al. (2018) in Section 4.2, and we contrast the performance of our bootstrapped variant (shown in Figure 4D) to the variant originally proposed in Tibshirani et al. (2018). First, let $\boldsymbol{\beta}$ denote $\overline{\theta}$, the grand mean of $\boldsymbol{\theta}$ (i.e., a 0-changepoint model). Then, the main idea in Tibshirani et al. (2018) is to approximate the law of $\boldsymbol{v}^T\boldsymbol{Y}$ used to construct the TG statistic (8) with the bootstrapped distribution of $\boldsymbol{v}^T(\boldsymbol{Y}-\boldsymbol{\beta})$ by bootstrapping the residuals, $\boldsymbol{y}-\overline{y}\cdot\mathbb{1}_n$. Here, the empirical grand mean $\overline{y}\cdot\mathbb{1}_n$ represents the simplest model with no changepoints for a length-n vector. While this estimate will usually ensure the resulting p-values has valid Type-I error control, we see that it produces overly conservative p-values in practice if there exist *any*

changepoints (Figure 9). Hence, as mentioned in Section 4.2, we suggest researchers to use the bootstrapping variant we proposed over the original method in Tibshirani et al. (2018), since it yields more powerful p-values and does not seem to violate the Type-I error control in practice.

[Figure 9 about here.]

G.3 *Additional details of Botton analysis in Section 4.3.* In this section, we provide additional details associated with the results in Section 4.3. The data for these analyses originated from `https://github.com/etal/cnvkit-examples`, the GitHub repository associated with Talevich et al. (2016). In our experience, our inferential tools work well on sequencing data as long as it is appropriately preprocessed. Specifically, we preprocessed our sequencing data using CNVkit according to the scripts within the CNVkit GitHub repository, which converts the BAM file containing the counts into the desired $\log_2$ copy number ratio, and applies sophisticated processing to correct for coverage biases. We then additionally filtered out outliers based on whether or not a particular data point lied outside of 1.5 times the interquantile range (IQR) of the median within a local window. This is done, as suggested by the documentation to the CNVkit pipeline. Since the resulting aCGH data is originally more than 7 times the length of the sequencing data (in terms of the number of probes used), we performed a down-sampling on the aCGH data by averaging each non-overlapping consecutive set of $\log_2$ values from 7 probes into one $\log_2$ value. This ensured that the number of samples for each chromosome was roughly comparable between sequencing and aCGH datasets. To use our inferential tools, we set σ^2 for all analyses on sequencing data by computing the standard deviation of the residuals after fitting a 5-step WBS model on each chromosome aside from chromosome 5 and 10. Similarly, we set σ^2 for all analyses on aCGH data by computing the standard deviation of the residuals after fitting a 0-changepoint model on each chromosome aside from chromosome 5 and 10. We used a 0-changepoint model for

the aCGH data since our diagnostics (similar to those done in Section 4.2) showed that the results were slightly heavy-tailed. Hence, as discussed in Appendix G.2, by fitting a 0-changepoint model, this empirically retains the Type-I error control at the cost of more conservative inference.

H *Proofs of results*

H.1 *Proof of Proposition 1, (BS).*

Proof. When $k = 1$, $2(n-2)$ linear inequalities characterize the single changepoint model $\{b_1, d_1\}$:

$$d_1 \cdot \boldsymbol{g}_{(1,b_1,n)}^T \boldsymbol{y} \geqslant \boldsymbol{g}_{(1,b,n)}^T \boldsymbol{y}, \quad \text{and} \quad d_1 \cdot \boldsymbol{g}_{(1,b_1,n)}^T \boldsymbol{y} \geqslant -\boldsymbol{g}_{(1,b,n)}^T \boldsymbol{y}, \quad b \in \{1, \ldots, n-1\} \backslash \{b_1\}.$$

Now by induction, assume we have constructed a polyhedral representation of the selection event up through step $k-1$. All that remains is to characterize the kth estimated changepoint and direction $\{b_k, d_k\}$ by inequalities that are linear in y. This can be done with $2(n-k-1)$ inequalities. To see this, assume without a loss of generality that the maximizing interval is $j_k = k$; then $\{b_k, d_k\}$ must satisfy the $2(|\boldsymbol{I}_k| - 2)$ inequalities

$$d_k \cdot \boldsymbol{g}_{(s_k,b_k,e_k)}^T \boldsymbol{y} \geqslant \boldsymbol{g}_{(s_k,b,e_k)}^T \boldsymbol{y} \quad \text{and} \quad d_k \cdot \boldsymbol{g}_{(s_k,b_k,e_k)}^T \boldsymbol{y} \geqslant -\boldsymbol{g}_{(s_k,b,e_k)}^T \boldsymbol{y}, \quad b \in \{s_k, \ldots, e_k - 1\} \backslash \{b_k\}.$$

For each interval $\boldsymbol{I}_\ell$, for $\ell = 1, \ldots, k-1$, we also have $2(|\boldsymbol{I}_\ell| - 1)$ inequalities

$$d_k \cdot \boldsymbol{g}_{(s_k,b_k,e_k)}^T \boldsymbol{y} \geqslant \boldsymbol{g}_{(s_\ell,b,e_\ell)}^T \boldsymbol{y} \quad \text{and} \quad d_k \cdot \boldsymbol{g}_{(s_k,b_k,e_k)}^T \boldsymbol{y} \geqslant -\boldsymbol{g}_{(s_\ell,b,e_\ell)}^T \boldsymbol{y}, \quad b \in \{s_\ell, \ldots, e_\ell - 1\}.$$

The last two displays together completely determine $\{b_k, d_k\}$, and as $\sum_{\ell=1}^k |\boldsymbol{I}_\ell| = n$, we get our desired total of $2(n-k-1)$ inequalities.

H.2 *Proof of Proposition 2, (WBS).*

Proof. The construction of $\boldsymbol{\Gamma}$ is basically the same as that for BS in Proposition 1; the only difference is that, at step k, the inequalities defining the new rows of $\boldsymbol{\Gamma}$ are based on the intervals w_{j_k} and w_ℓ, $\ell \in J_k \backslash \{j_k\}$, instead of $\boldsymbol{I}_{j_k}$ and $\boldsymbol{I}_\ell$, $\ell \neq j_k$, respectively. To compute the

upper bound on the number of rows m, observe that in step $\ell \in \{1, \ldots, k\}$, there are at most $B - \ell + 1$ intervals remaining. Among these, the interval j_k contributes $p - 2$ inequalities, and the remaining $B - \ell$ intervals contributes $p - 1$ inequalities.

H.3 *Proof of Proposition 1, (CBS).*

Proof. The proof follows similarly to the proof of Proposition 1. Observe that for any $k' < k$, the model $M^{\text{CBS}}_{1:k'}(\boldsymbol{y}_{\text{obs}})$ is strictly contained in the model $M^{\text{CBS}}_{1:k}(\boldsymbol{y}_{\text{obs}})$. Hence, we can proceed using induction, and let b_i for $i \in \{1, \ldots, k\}$ denote $\widehat{b}_i$ for simplicity, and do the same for a_i, d_i and j_i. Let $C(x, 2) = \binom{x}{2}$ for simplicity as well.

For $k = 1$, the following $2 \cdot (C(n-1, 2) - 1)$ inequalities characterize the selection of the changepoint model $\{a_1, b_1, d_1\}$,

$$d_1 \cdot \boldsymbol{g}^T_{(1,a_1,b_1,n)}\boldsymbol{y} \geqslant \boldsymbol{g}^T_{(1,r,t,n)}\boldsymbol{y}, \quad \text{and} \quad d_1 \cdot \boldsymbol{g}^T_{(1,a_1,b_1,n)}\boldsymbol{y} \geqslant -\boldsymbol{g}^T_{(1,r,t,n)}\boldsymbol{y},$$

for all $r, t \in \{1, \ldots, n-1\}$ where $r < t$, $r \neq a_1$ and $t \neq b_1$.

By induction, assume we have constructed the polyhedra for the model, $M^{\text{CBS}}_{1:(k-1)}(\boldsymbol{y}_{\text{obs}}) = \{\boldsymbol{a}_{1:(k-1)}, \boldsymbol{b}_{1:(k-1)}, \boldsymbol{d}_{1:(k-1)}\}$. To construct $M^{\text{CBS}}_{1:k}(\boldsymbol{y}_{\text{obs}})$, all that remains is to characterize the kth parameters $\{a_k, b_k, d_k\}$. To do this, assume that j_k corresponds with the interval $\boldsymbol{I}_k$ having the form $\{s_k, \ldots, e_k\}$. Within this interval, we form the first $2 \cdot (C(|\boldsymbol{I}_{j_k}| - 1, 2) - 1)$ inequalities of the form,

$$d_k \cdot \boldsymbol{g}^T_{(s_k,a_k,b_k,e_k)}\boldsymbol{y} \geqslant \boldsymbol{g}^T_{(s_k,r,t,e_k)}\boldsymbol{y} \quad \text{and} \quad d_k \cdot \boldsymbol{g}^T_{(s_k,a_k,b_k,e_k)}\boldsymbol{y} \geqslant -\boldsymbol{g}^T_{(s_k,r,t,e_k)}\boldsymbol{y}$$

for all $r, t \in \{s_k, \ldots, e_k - 1\}$ where $r < t$ and $r \neq a_k$ and $t \neq b_k$. The remaining inequalities originate from the remaining intervals. For each interval $\boldsymbol{I}_\ell$, for $\ell \in \{1, \ldots, 2k-1\} \backslash \{j_k\}$, let $\boldsymbol{I}_\ell$ have the form $\{s_\ell, \ldots, e_\ell\}$. We form the next $2 \cdot C(|\boldsymbol{I}_\ell| - 1, 2)$ inequalities of the form

$$d_k \cdot \boldsymbol{g}^T_{(s_k,a_k,b_k,e_k)}\boldsymbol{y} \geqslant \boldsymbol{g}^T_{(s_\ell,r,t,e_\ell)}y \quad \text{and} \quad d_k \cdot \boldsymbol{g}^T_{(s_k,a_k,b_k,e_k)}\boldsymbol{y} \geqslant -\boldsymbol{g}^T_{(s_\ell,r,t,e_\ell)}\boldsymbol{y}$$

for all $r, t \in \{s_\ell, \ldots, e_\ell - 1\}$ where $r < t$.

H.4 *Proof of Proposition 3, (Marginalization).*

Proof. For concreteness, we write the proof where $\boldsymbol{W}$ represents additive noise, but the proof generalizes to the setting where $\boldsymbol{W}$ represents random intervals easily. First write $T(\boldsymbol{y}_{\text{obs}}, \boldsymbol{v})$ as an integral over the joint density of $\boldsymbol{W}$ and $\boldsymbol{Y}$,

$$\begin{aligned} T(\boldsymbol{y}_{\text{obs}}, \boldsymbol{v}) &= P(\boldsymbol{v}^T\boldsymbol{Y} \geqslant \boldsymbol{v}^T\boldsymbol{y}_{\text{obs}} | M(\boldsymbol{Y}+\boldsymbol{W}) = M(\boldsymbol{y}_{\text{obs}}+\boldsymbol{W}), \Pi_{\boldsymbol{v}}^{\perp}\boldsymbol{Y} = \Pi_{\boldsymbol{v}}^{\perp}\boldsymbol{y}_{\text{obs}}) \\ &= \int \mathbb{1}(\boldsymbol{v}^T\boldsymbol{y} \geqslant \boldsymbol{v}^T\boldsymbol{y}_{\text{obs}}) f_{\boldsymbol{W},\boldsymbol{Y}|E_1,E_2}(\boldsymbol{w},\boldsymbol{y}) d\boldsymbol{w} d\boldsymbol{y}. \end{aligned} \tag{17}$$

Then the joint density $f_{\boldsymbol{W},\boldsymbol{Y}|E_1,E_2}(\boldsymbol{w},\boldsymbol{y})$ partitions into two components, whose latter component (a probability mass function) can be rewritten using Bayes rule. For convenience, denote $g(\boldsymbol{w}) = \mathbb{P}(E_1|\boldsymbol{W}=\boldsymbol{w}, E_2)$.

$$\begin{aligned} f_{\boldsymbol{W},\boldsymbol{Y}|E_1,E_2}(\boldsymbol{w},\boldsymbol{y}) d\boldsymbol{y} d\boldsymbol{w} &= f_{\boldsymbol{Y}|\boldsymbol{W}=\boldsymbol{w},E_1,E_2}(\boldsymbol{y}) \cdot f_{\boldsymbol{W}|E_1,E_2}(\boldsymbol{w})\ d\boldsymbol{y}\ d\boldsymbol{w} \\ &= f_{\boldsymbol{Y}|\boldsymbol{W}=\boldsymbol{w},E_1,E_2}(\boldsymbol{y}) \cdot \frac{\mathbb{P}(E_1|\boldsymbol{W}=\boldsymbol{w},E_2) f_{\boldsymbol{W}|E_2}(\boldsymbol{w})}{\mathbb{P}(E_1|E_2)}\ d\boldsymbol{y}\ d\boldsymbol{w} \\ &= f_{\boldsymbol{Y}|\boldsymbol{W}=\boldsymbol{w},E_1,E_2}(\boldsymbol{y}) \cdot \frac{g(\boldsymbol{w}) f_{\boldsymbol{W}}(\boldsymbol{w})}{\int g(\boldsymbol{w}') f_{\boldsymbol{W}}(\boldsymbol{w}') d\boldsymbol{w}'}\ d\boldsymbol{y}\ d\boldsymbol{w}, \end{aligned}$$

where we used the independence between W and E_2 in the last equality. With this, $T(\boldsymbol{y}_{\text{obs}}, \boldsymbol{v})$ from (17) becomes:

$$T(\boldsymbol{y}_{\text{obs}}, \boldsymbol{v}) = \int \mathbb{1}(\boldsymbol{v}^T\boldsymbol{y} \geqslant \boldsymbol{v}^T\boldsymbol{y}_{\text{obs}}) \cdot g(\boldsymbol{w}) \cdot \frac{f_{\boldsymbol{W}|E_2}(\boldsymbol{w})}{\int g(\boldsymbol{w}') f_{\boldsymbol{W}}(\boldsymbol{w}') d\boldsymbol{w}'} \cdot f_{\boldsymbol{Y}|\boldsymbol{W}=\boldsymbol{w},E_1,E_2}(\boldsymbol{y})\ d\boldsymbol{y}\ d\boldsymbol{w}.$$

Now, rearranging, we get:

$$\begin{aligned} T(\boldsymbol{y}_{\text{obs}}, \boldsymbol{v}) &= \int \underbrace{\left\{ \int \mathbb{1}(\boldsymbol{v}^T\boldsymbol{y} \geqslant \boldsymbol{v}^T\boldsymbol{y}_{\text{obs}}) \cdot f_{\boldsymbol{Y}|\boldsymbol{W}=\boldsymbol{w},E_1,E_2}(\boldsymbol{y}) d\boldsymbol{y} \right\}}_{T(\boldsymbol{y}_{\text{obs}},\boldsymbol{v},\boldsymbol{w})} \underbrace{\frac{g(\boldsymbol{w})}{\int g(\boldsymbol{w}') f_{\boldsymbol{W}}(\boldsymbol{w}') d\boldsymbol{w}'}}_{a(\boldsymbol{w})} f_{\boldsymbol{W}}(\boldsymbol{w}) d\boldsymbol{w} \\ &= \int T(\boldsymbol{y}_{\text{obs}}, \boldsymbol{v}, \boldsymbol{w}) a(\boldsymbol{w})\ f_{\boldsymbol{W}}(\boldsymbol{w})\ d\boldsymbol{w}. \end{aligned} \tag{18}$$

This proves the first equality in Proposition 3. To show what the weighting factor $a(\boldsymbol{w})$ equals, observe that by applying Bayes rule to the numerator of $a(\boldsymbol{w}_{\text{obs}})$, and rearranging:

$$\begin{aligned} a(\boldsymbol{w}) &= \frac{g(\boldsymbol{w})}{\int g(\boldsymbol{w}') f_W(\boldsymbol{w}')\ d\boldsymbol{w}'} = \frac{\mathbb{P}(E_1|E_2, \boldsymbol{W}=\boldsymbol{w})}{P(E_1|E_2)} = \frac{\mathbb{P}(\boldsymbol{W}=\boldsymbol{w}|E_1,E_2)}{\mathbb{P}(\boldsymbol{W}=\boldsymbol{w}|E_2)} \\ &= \frac{\mathbb{P}(\boldsymbol{W}=\boldsymbol{w}|E_1,E_2)}{\mathbb{P}(\boldsymbol{W}=\boldsymbol{w})}. \end{aligned}$$

Finally, to show the second equality in Proposition 3, observe that we can also represent

$a(\boldsymbol{w})$ as

$$a(\boldsymbol{w}) = \frac{g(\boldsymbol{w})}{\mathbb{E}[g(\boldsymbol{w})]} \tag{19}$$

by definition, where the denominator is the expectation taken with respect to the random variable $\boldsymbol{W}$. Leveraging the geometric theorems in works like Tibshirani et al. (2018), it can be shown that

$$g(\boldsymbol{w}) = P\Big(M(\boldsymbol{Y}+\boldsymbol{W}) = M(\boldsymbol{y}_{\text{obs}}+\boldsymbol{W}) \mid \Pi_{\boldsymbol{v}}^{\perp}\boldsymbol{Y} = \Pi_{\boldsymbol{v}}^{\perp}\boldsymbol{y}_{\text{obs}}\Big) = \Phi(\mathcal{V}_{\text{up}}/\tau) - \Phi(\mathcal{V}_{\text{lo}}/\tau). \tag{20}$$

Also from the same references as well as stated in Section 3.3, we know that

$$T(\boldsymbol{y}_{\text{obs}}, \boldsymbol{v}, \boldsymbol{w}) = \frac{\Phi(\mathcal{V}_{\text{up}}/\tau) - \Phi(\boldsymbol{v}^T\boldsymbol{y}_{\text{obs}}/\tau)}{\Phi(\mathcal{V}_{\text{up}}/\tau) - \Phi(\mathcal{V}_{\text{lo}}/\tau)} \tag{21}$$

Putting (19), (20) and (21) together into (18), we complete the proof by obtaining

$$T(\boldsymbol{y}_{\text{obs}}, \boldsymbol{v}) = \frac{\int T(\boldsymbol{y}_{\text{obs}}, \boldsymbol{v}, \boldsymbol{w}) g(\boldsymbol{w}) f_{\boldsymbol{W}}(\boldsymbol{w}) d\boldsymbol{w}}{\int g(\boldsymbol{w}) f_{\boldsymbol{W}}(\boldsymbol{w}) d\boldsymbol{w}} = \frac{\int \Phi(\mathcal{V}_{\text{up}}/\tau) - \Phi(\boldsymbol{v}^T\boldsymbol{y}_{\text{obs}}/\tau) f_{\boldsymbol{W}}(\boldsymbol{w}) d\boldsymbol{w}}{\int \Phi(\mathcal{V}_{\text{up}}/\tau) - \Phi(\mathcal{V}_{\text{lo}}/\tau) f_{\boldsymbol{W}}(\boldsymbol{w}) d\boldsymbol{w}}.$$

References

Fithian, W., Taylor, J., Tibshirani, R., and Tibshirani, R. J. (2015). Selective sequential model selection. arXiv: 1512.02565.

Hyun, S., G'Sell, M., and Tibshirani, R. J. (2018). Exact post-selection inference for the generalized lasso path. *Electronic Journal of Statistics* pages 1053–1097.

Lin, K., Sharpnack, J. L., Rinaldo, A., and Tibshirani, R. J. (2017). A sharp error analysis for the fused lasso, with application to approximate changepoint screening. In *Advances in Neural Information Processing Systems*, pages 6884–6893.

Olshen, A., Seshan, V. E., Lucito, R., and Wigler, M. (2004). Circular binary segmentation for the analysis of array-based DNA copy number data. *Biostatistics* **5,** 557–572.

Snijders, A. M., Nowak, N., Segraves, R., Blackwood, S., Brown, N., Conroy, J., Hamilton, G., Hindle, A. K., Huey, B., Kimura, K., et al. (2001). Assembly of microarrays for genome-wide measurement of DNA copy number. *Nature genetics* **29,** 263–264.

Talevich, E., Shain, A. H., Botton, T., and Bastian, B. C. (2016). CNVkit: Genome-wide copy number detection and visualization from targeted DNA sequencing. *PLoS computational biology* **12,**.

Tibshirani, R. J., Rinaldo, A., Tibshirani, R., and Wasserman, L. (2018). Uniform asymptotic inference and the bootstrap after model selection. *Ann. Statist.* **46,** 1255–1287.

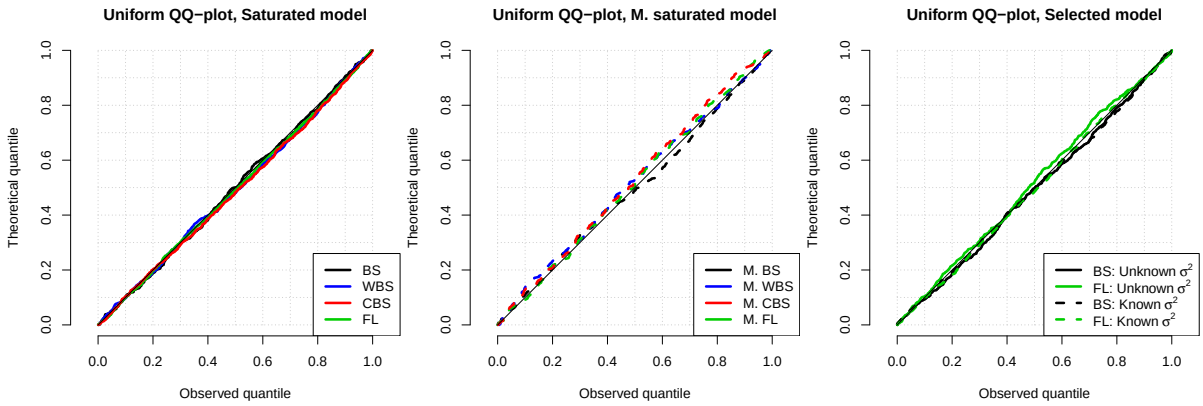

Figure 1: *All plots showing the p-values of various statistical inferences under the global null. (Left): Saturated model tests, specifically BS (black), WBS (blue), CBS (red) and FL (green). (Middle): Marginalized variants of the left plot. (Right): Selected model tests, specifically BS (black) and FL (green), either with unknown* σ^2 *(solid) or known* σ^2 *(dashed). Note: this figure appears in color in the electronic version of this article, and any mention of color refers to that version.*

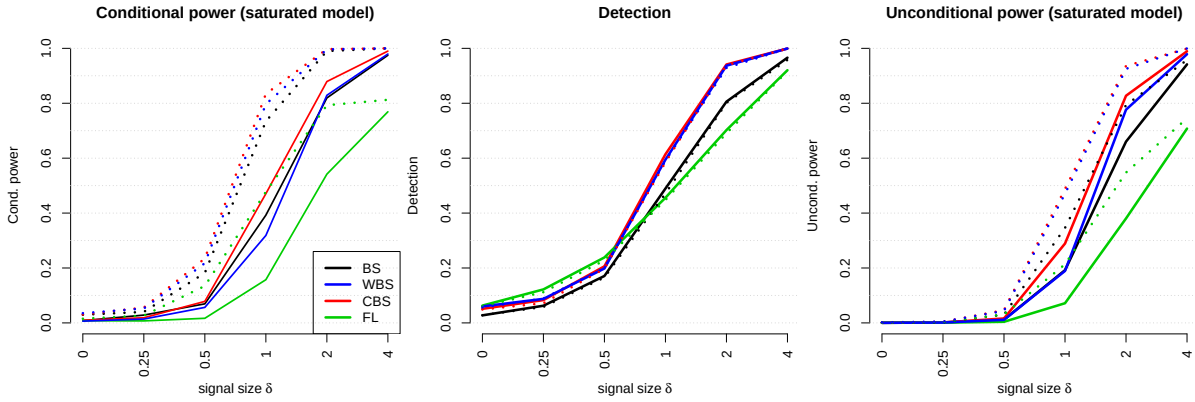

Figure 2: *Data was simulated from two settings over signal size* $\delta \in (0, 4)$ *with* $n = 200$ *data points. Several two-step algorithms (WBS, SBS, CBS, FL) were applied, and post-selection segment test inference was conducted on the resulting two detected changepoints from each method. The dotted lines are the marginalized versions of each test. Note: this figure appears in color in the electronic version of this article, and any mention of color refers to that version.*

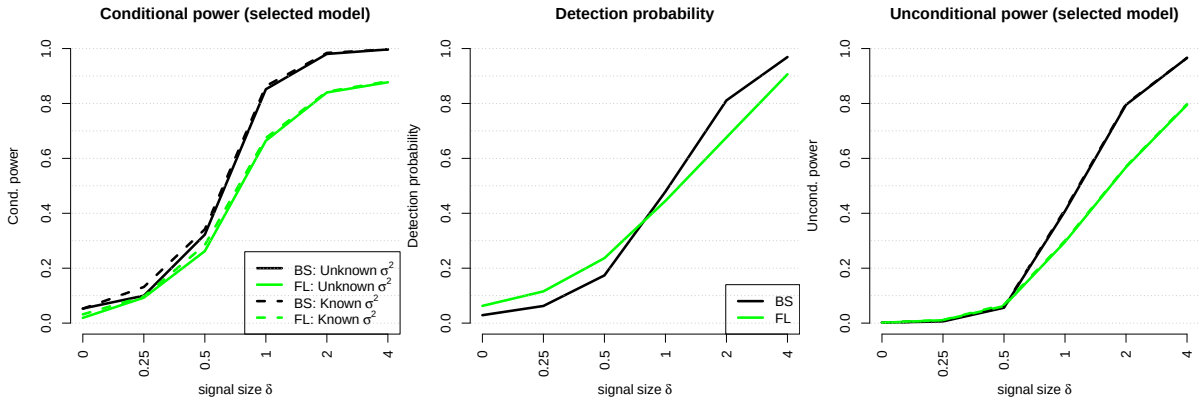

Figure 3: *Setup similar to Figure 2 but for selected model tests. Only BS (black) and FL (green) are shown. but the selected model test is applied to both known (dashed line) and unknown noise parameter σ^2 (solid line). Note: this figure appears in color in the electronic version of this article, and any mention of color refers to that version.*

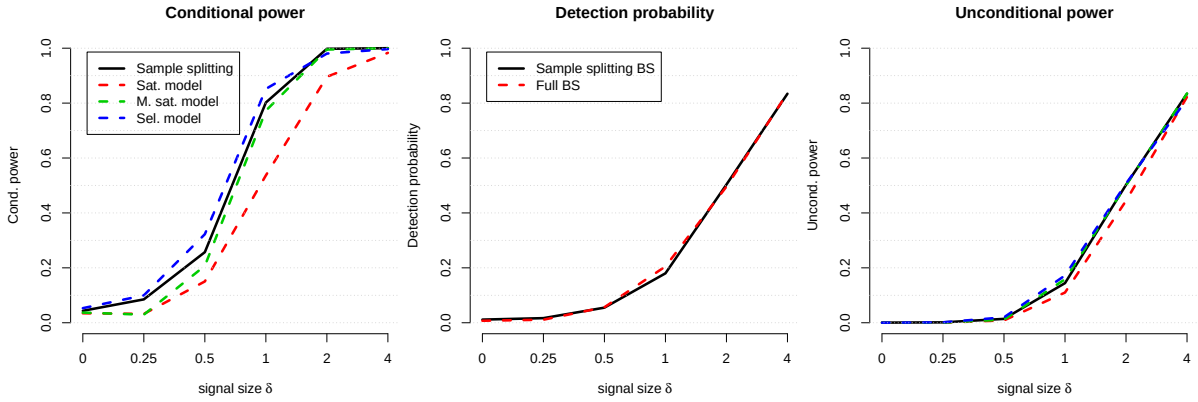

Figure 4: *The same setup as in Figure 2 but with exact detection. Note: this figure appears in color in the electronic version of this article, and any mention of color refers to that version.*

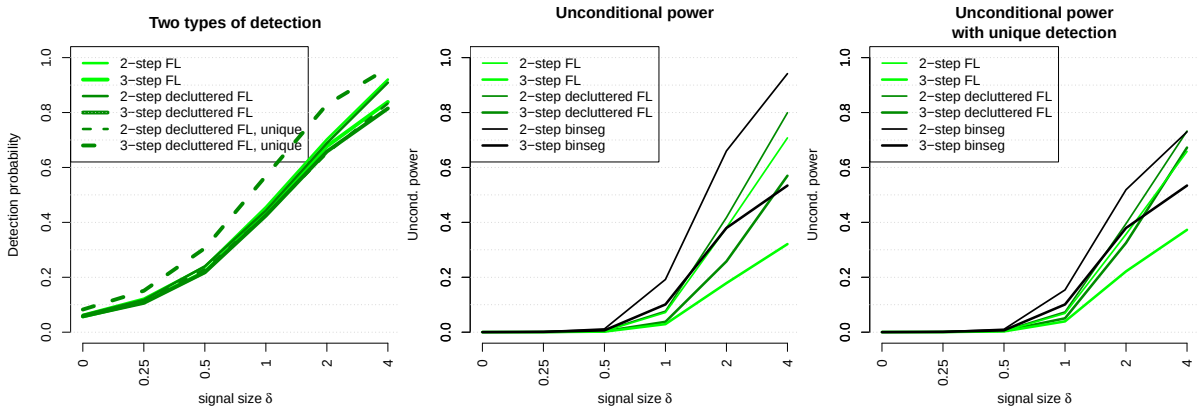

Figure 5: *(Left): Various detections for FL, either using 2 or 3 steps, and either using decluttering or not. (Middle): The unconditional power of various segmentation algorithms. (Right): The unconditional power, but defined as the conditional power multiplied by the unique detection probability. Note: this figure appears in color in the electronic version of this article, and any mention of color refers to that version.*

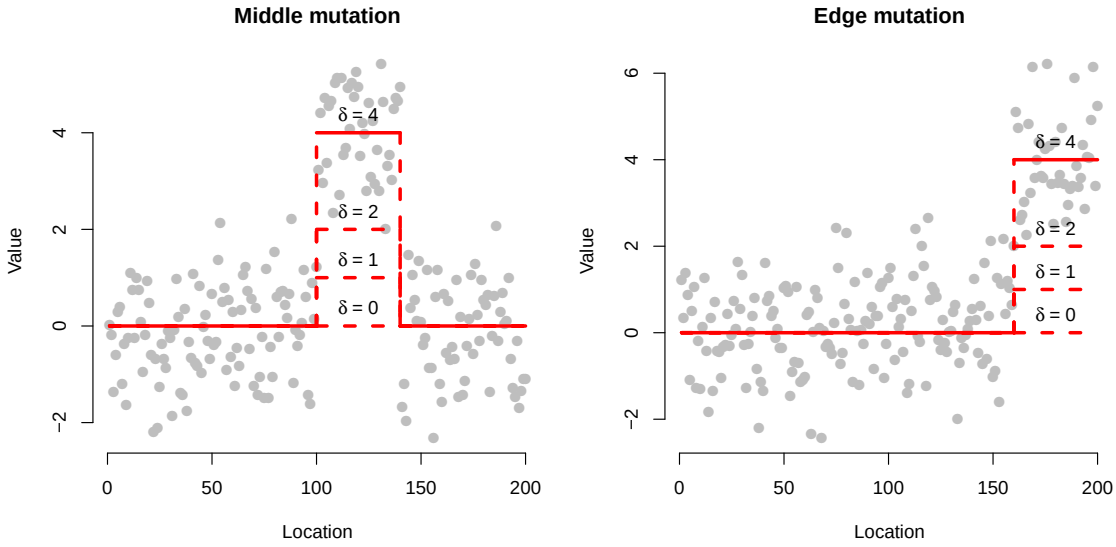

Figure 6: *(Left) Example of simulated Gaussian data for middle mutation as defined in* (9) *with* $\delta = 4$*, with data length* $n = 200$ *and noise level* $\sigma = 1$*. The possible mean vectors* θ *for* $\delta = 0, 1, 2$ *are also shown. (Right) Analogous to the left figure, but representing edge mutations defined in* (14)*. Note: this figure appears in color in the electronic version of this article, and any mention of color refers to that version.*

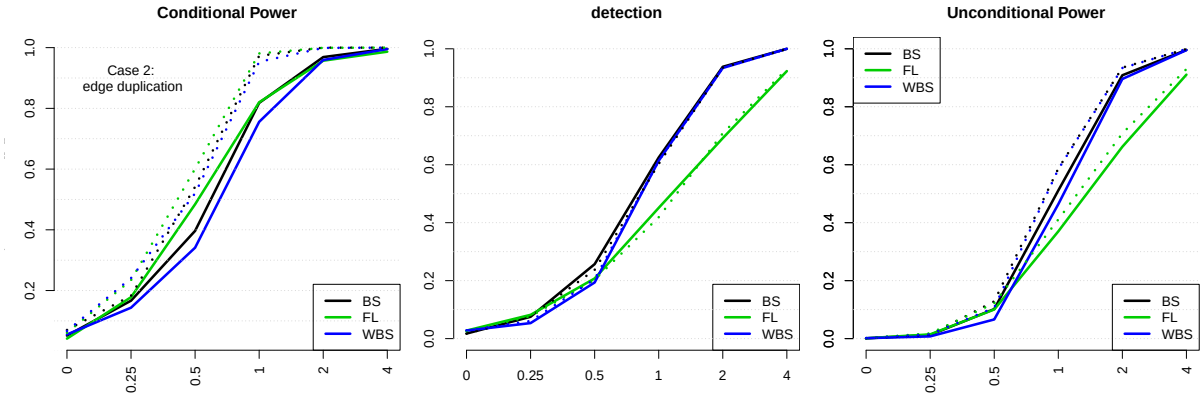

Figure 7: *Same setup as Figure 2 but for edge-mutation data. Note: this figure appears in color in the electronic version of this article, and any mention of color refers to that version.*

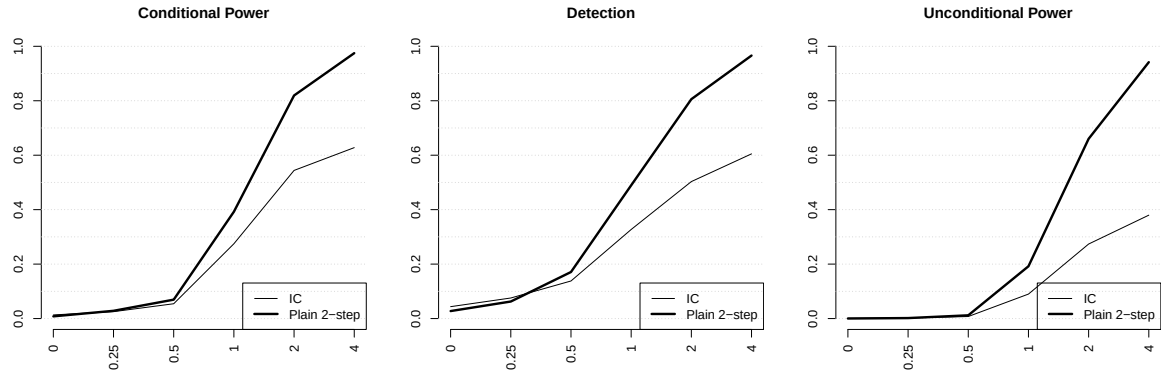

Figure 8: *Similar setup as Figure 2. In the middle-mutation data example from (9). IC-stopped BS inference (bold line) is compared to a fixed 2-step BS inference (thin line). We can see that the power and detection are considerably lower. The average number of steps taken per each* δ *on x-axis ticks are* $1.34, 1.86, 3.02, 3.64, 3.77, 3.72$*, respectively.*

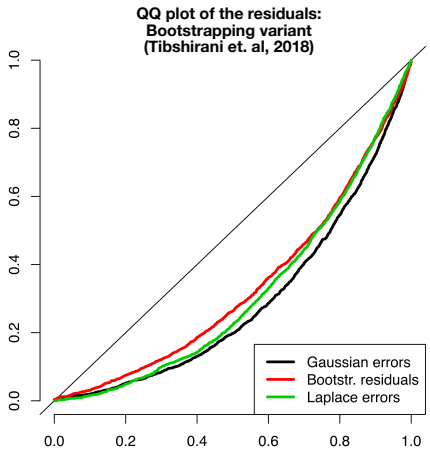

Figure 9: *QQ-plot of p-values derived from the bootstrap substitution method developed in Tibshirani et al. (2018). These results are presented in a similar fashion to Figure 4 C and D. Note: this figure appears in color in the electronic version of this article, and any mention of color refers to that version.*